

CCSITM
Carbon Capture Simulation Initiative

NETL ARRA Report on the Development of a Dynamic Simulation of a Solid Sorbent Capture Process and Controllability Assessment

Prepared by
Dr. Debangsu Bhattacharyya
Dr. Srinivasarao Modekurti
Department of Chemical Engineering
West Virginia University
Morgantown, WV 26506, USA

In collaboration with
Stephen E. Zitney
National Energy Technology Laboratory

Prepared for
U.S. Department of Energy
National Energy Technology Laboratory

02/21/2012



Revision Log

Revision	Date	Revised By:	Description
0	01/26/2012	Dr. Debangsu Bhattacharyya (WVU) Dr. Srinivasarao Modekurti (WVU)	Original
1	02/15/2012	Dr. Stephen E. Zitney (NETL)	Review
2	02/21/2012	Dr. Stephen E. Zitney (NETL)	Use updated cover page and header; Added Acknowledgement of Funding
3	2/22/2012		Updated title, task set reference

Disclaimer

This report was prepared as an account of work sponsored by an agency of the United States Government.

Neither the United States Government nor any agency thereof, nor any of their employees, makes any warranty, express or implied, or assumes any legal liability or responsibility for the accuracy, completeness, or usefulness of any information, apparatus, product, or process disclosed, or represents that its use would not infringe privately owned rights. Reference herein to any specific commercial product, process, or service by trade name, trademark, manufacturer, or otherwise does not necessarily constitute or imply its endorsement, recommendation, or favoring by the United States Government or any agency thereof. The views and opinions of authors expressed herein do not necessarily state or reflect those of the United States Government or any agency thereof.

Acknowledgement of Funding

This project was funded under the Carbon Capture Simulation Initiative under the following FWP's and contracts:

LANL - FE-101-002-FY10

PNNL - 60115

LLNL - FEW0180

LBNL - CSNW1130

NETL - RES-0004000.6.600.007.002

Table of Contents

1.0	Background.....	1-21
2.0	Model development	2-1
3.0	Results and discussion	3-1
4.0	Future plan of work	4-1
5.0	References.....	5-1

List of Figures

Figure 2-1	Schematic of a single stage adsorber reactor (a) overflow-type (b) underflow-type	2.1-3
Figure 2-2	Schematic of a two-stage adsorber reactor.....	2.1-3
Figure 2-3	Process flow diagram for the CO ₂ compression system	2.2-4

Single stage adsorber - overflow type

Figure 3-1	Dynamics of the bubble phase temperature at the exit of the adsorber as a result of 20 kmol/hr step increase in the flue gas flowrate.....	Error! Bookmark not defined. 3-1
Figure 3-2	Dynamics of the emulsion phase solids temperature at the exit of the adsorber as a result of 20 kmol/hr step increase in the flue gas flowrate	3-2
Figure 3-3	Dynamics of the CO ₂ concentration at the exit of the adsorber as a result of 20 kmol/hr step increase in the flue gas flowrate	3-2
Figure 3-4	Dynamics of the bubble phase temperature at the exit of the adsorber as a result of 4°C step increase in the solids inlet temperature	3-3
Figure 3-5	Dynamics of the emulsion phase solids temperature at the exit of the adsorber as a result of 4°C step increase in the solids inlet temperature	3-3
Figure 3-6	Dynamics of the CO ₂ concentration at the exit of the adsorber as a result of 4°C step increase in the solids inlet temperature	3-4
Figure 3-7	Dynamics of the bubble phase temperature at the exit of the adsorber as a result of 5% step increase in the solids flowrate	3-4
Figure 3-8	Dynamics of the emulsion phase temperature at the exit of the adsorber as a result of 5% step increase in the solids flowrate	3-5

Figure 3-9 Dynamics of the CO ₂ concentration at the exit of the adsorber as a result of 5% step increase in the solids flowrate	3-5
Figure 3-10 Dynamics of the bubble phase temperature at the exit of the adsorber as a result of 10% step increase in the mole fraction of CO ₂ in the flue gas inlet flowrate	3-6
Figure 3-11 Dynamics of the emulsion phase temperature at the exit of the adsorber as a result of 10% step increase in the mole fraction of CO ₂ in the flue gas inlet flowrate.....	3-6
Figure 3-12 Dynamics of the CO ₂ concentration at the exit of the adsorber as a result of 10% step increase in the mole fraction of CO ₂ in the flue gas inlet flowrate	3-7

Single stage adsorber – under-flow type

Figure 3-13 Dynamics of the bubble phase temperature at the exit of the adsorber as a result of 20 kmol/hr step increase in the flue gas flowrate.....	Error! Bookmark not defined.8
Figure 3-14 Dynamics of the emulsion phase solids temperature at the exit of the adsorber as a result of 20 kmol/hr step increase in the flue gas flowrate	Error! Bookmark not defined.8
Figure 3-15 Dynamics of the CO ₂ concentration at the exit of the adsorber as a result of 20 kmol/hr step increase in the flue gas flowrate	Error! Bookmark not defined.9
Figure 3-16 Dynamics of the bubble phase temperature at the exit of the adsorber as a result of 4°C step increase in the solids inlet temperature	Error! Bookmark not defined.9
Figure 3-17 Dynamics of the emulsion phase solids temperature at the exit of the adsorber as a result of 4°C step increase in the solids inlet temperature ...	Error! Bookmark not defined.0
Figure 3-18 Dynamics of the CO ₂ concentration at the exit of the adsorber as a result of 4°C step increase in the solids inlet temperature	Error! Bookmark not defined.0
Figure 3-19 Dynamics of the bubble phase temperature at the exit of the adsorber as a result of 5% step increase in the solids flowrate	Error! Bookmark not defined.1
Figure 3-20 Dynamics of the emulsion phase temperature at the exit of the adsorber as a result of 5% step increase in the solids flowrate.....	Error! Bookmark not defined.1
Figure 3-21 Dynamics of the CO ₂ concentration at the exit of the adsorber as a result of 5% step increase in the solids flowrate	Error! Bookmark not defined.2
Figure 3-22 Dynamics of the bubble phase temperature at the exit of the adsorber as a result of 10% step increase in the mole fraction of CO ₂ in the flue gas inlet flowrate	Error! Bookmark not defined.2
Figure 3-23 Dynamics of the emulsion phase temperature at the exit of the adsorber as a result of 10% step increase in the mole fraction of CO ₂ in the flue gas inlet flowrate	Error! Bookmark not defined.2

Figure 3-24 Dynamics of the CO₂ concentration at the exit of the adsorber as a result of 10% step increase in the mole fraction of CO₂ in the flue gas inlet flowrate..... **Error! Bookmark not defined.**

Two- stage adsorber

Figure 3-25 Dynamics of the bubble phase temperature at the exit of the stage 1 as a result of 5% step increase in the solids flowrate 3-14

Figure 3-26 Dynamics of the bubble phase temperature at the exit of the stage 2 as a result of 5% step increase in the solids flowrate 3-15

Figure 3-27 Dynamics of the emulsion phase temperature at the exit of the stage 1 as a result of 5% step increase in the solids flowrate 3-15

Figure 3-28 Dynamics of the emulsion phase temperature at the exit of the stage 2 as a result of 5% step increase in the solids flowrate 3-16

Figure 3-29 Dynamics of the CO₂ concentration at the exit of the stage 1 as a result of 5% step increase in the solids flowrate 3-16

Figure 3-30 Dynamics of the CO₂ concentration at the exit of the stage 2 as a result of 5% step increase in the solids flowrate 3-17

Figure 3-31 Dynamics of the bubble phase temperature at the exit of the stage 1 as a result of 4°C step increase in the solids inlet temperature 3-17

Figure 3-32 Dynamics of the bubble phase temperature at the exit of the stage 2 as a result of 4°C step increase in the solids inlet temperature 3-18

Figure 3-33 Dynamics of the emulsion phase solids temperature at the exit of the stage 1 as a result of 4°C step increase in the solids inlet temperature 3-18

Figure 3-34 Dynamics of the emulsion phase solids temperature at the exit of the stage 2 as a result of 4°C step increase in the solids inlet temperature 3-19

Figure 3-35 Dynamics of the CO₂ concentration at the exit of the stage 1 as a result of 4°C step increase in the solids inlet temperature 3-19

Figure 3-36 Dynamics of the CO₂ concentration at the exit of the stage 2 as a result of 4°C step increase in the solids inlet temperature 3-20

Pressure-driven dynamic simulation of the CO₂ compression system

Figure 3-37 Step change in the inlet pressure of the CO ₂ -rich stream	3-21
Figure 3-38 Transients in the inlet flowrate due to step change in the inlet pressure.....	3-21
Figure 3-39 Transients in the outlet pressure of the LP section due to step increase in the inlet pressure	3-22
Figure 3-40 Transients in the outlet pressure of the MP section due to step increase in the inlet pressure	3-22
Figure 3-41 Transients in the discharge of the second stage in the HP section due to step increase in the inlet pressure	3-23
Figure 3-42 Increase in the total power requirement due to step increase in the inlet pressure	3-23
Figure 3-43 Step decrease in the inlet pressure of the CO ₂ -rich stream	3-24
Figure 3-44 Transients in the inlet flowrate due to step decrease in the inlet pressure	3-24
Figure 3-45 Transients in the outlet pressure of the LP section due to step decrease in the inlet pressure	3-25
Figure 3-46 Transients in the outlet pressure of the MP section due to step decrease in the inlet pressure	3-25
Figure 3-47 Transients in the discharge of the second stage in the HP section due to step decrease in the inlet pressure	3-26
Figure 3-48 Decrease in the total power requirement due to step decrease in the inlet pressure	3-26
Figure 3-49 Step decrease in the CO ₂ concentration at the inlet.....	3-27
Figure 3-50 Transients in the inlet flowrate.....	3-28
Figure 3-51 Transients in the outlet pressure of the LP section due to step decrease in the CO ₂ concentration.....	3-28
Figure 3-52 Transients in the outlet pressure of the MP section due to step decrease in the CO ₂ section	3-29
Figure 3-53 Transients in the discharge of the second stage in the HP section due to step decrease in CO ₂ concentration.....	3-29
Figure 3-54 Transients in the discharge temperature of the HP section (before the cooler) due to decrease in CO ₂ concentration	3-30

Figure 3-55 Transients of the total power requirement due to step decrease in the CO₂ concentration..... 3-30

List of Tables

Table 4-1 Target dates 4-2

1.0 Background

Task Set 4 is focused on the operation and control of power plants with post-combustion CO₂ capture. Even though there are number of technologies for CO₂ capture [1-3], we are currently evaluating solid-sorbent [e.g., 4] CO₂ capture technology using dynamic simulation as the main computational tool.

Dynamic simulation is a highly sophisticated and powerful computational approach that can be used to help achieve aggressive operation and control objectives for CO₂ capture technologies. Dynamic simulation tools provide a continuous view of a process in action by calculating its transient behavior over time. Typical applications include normal and faulted operations, as well as process startup, upsets, and shutdown. Dynamic simulation can also be used to determine key equipment response times and to investigate interactions between major plant sections, such as power generation and CO₂ capture and compression. In addition, dynamic simulation can be used to evaluate alternative control strategies without the expense and the unexpected hazards of plant experimentation. Advanced process control (APC) strategies can also be applied to drive power production to satisfy load demands while meeting energy plant integration, performance, and environmental objectives, including CO₂ capture.

Task Set 4 is developing innovative dynamic simulation models, methods, and tools to address key operational and control challenges for new carbon capture technologies for which little or no operating experience is available. In Year 1, the main focus was on development of a flow-driven dynamic model of a bubbling-bed solid-sorbent adsorber and development of a pressure-driven dynamic model of a CO₂ compression system. In this annual report, the development of the dynamic models using the commercial Aspen Engineering Suite products, Aspen Plus, Aspen Custom Modeler, and Aspen Plus Dynamics, is described, followed by presentation of the results that were generated using these models.

2.0 Model Development

In Year 1, the overall objective was to develop dynamic models of the solid-sorbent CO₂ capture adsorber and the CO₂ compression system. The steady-state models obtained from Task Set 3 were modified to develop these dynamic models. The steady-state operating conditions and the model parameters were not modified. The main tasks in development of these dynamic models include consideration of the accumulation terms for the differential variables, modifications of the boundary conditions, if any, for the dynamic simulation, generation of consistent initial conditions, equipment sizing and heat transfer options wherever needed, development of a valid pressure-flow network, and any additional equations to capture the transients in the state variables. The dynamic models are then used for performing transient studies. These tasks will be described in more detail in the following sections.

2.1 Task 4.2.1a: Develop Dynamic Module for CO₂ Capture Reactor

This dynamic model is developed based on the steady-state model of the bubbling fluidized bed for solid-sorbent CO₂ capture developed by Task Set 3 [5]. The steady-state model was developed based on the open literature [6-7] using Aspen Custom Modeler (ACM) [8]. A thorough review of all the equations in the steady-state model has been done and the units of measurement have been checked for consistency. Scaling of the equations and variables and overall modeling methodology has been discussed with the Task Set 3 team. The steady-state model has been converted to a flow-driven dynamic model in ACM. This includes consideration of the hold-up terms in the differential equations along with consistent boundary conditions for a dynamic simulation. The derivatives of the state variables have been initialized to zero. Dynamics of the bubble phase temperature, sorbent temperature, and CO₂ concentration have been studied using the flow-driven dynamic model by introducing step changes in a number of manipulated and disturbance variables such as the flue gas flow rate, solids flow rate, and solids inlet temperature. The results are discussed in the next section. The observed transient trends are in good agreement with the expected behavior. However, some of these trends might change with pressure-driven dynamic simulations. Transient simulations have been performed with single-stage adsorbers (overflow-type and underflow-type) and a two-stage adsorber. Here, overflow means that the solids leave the stage by flowing over the overflow-weir. In the underflow-type configuration, the solids flow through the holes of the supporting tray. In a two-stage adsorber, underflow-type configuration has been considered for the upper stage and overflow-type configuration has been considered for the lower stage. The schematics of the single-stage adsorbers and two-stage adsorber are shown in Figures 2-1 and 2-2, respectively.

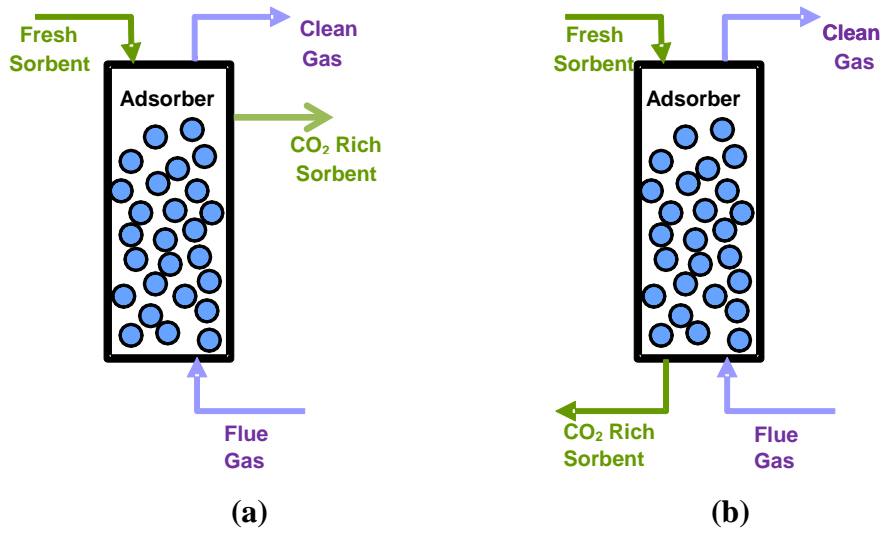


Figure 2-1 Schematic of a single stage adsorber reactor (a) overflow-type (b) underflow-type

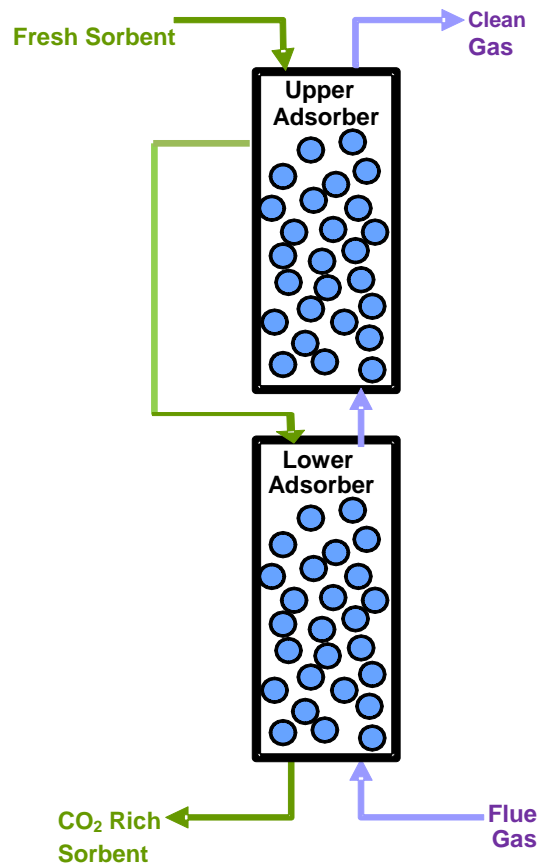


Figure 2-2 Schematic of a two-stage adsorber reactor

2.2 Task 4.2.2: Develop Dynamic Module for CO₂ Compression

In this task, the steady-state Aspen Plus model of the CO₂ compression system developed by Task Set 3 [9] was converted to a pressure-driven Aspen Plus Dynamics model. The Aspen Plus model was suitably modified for developing a valid pressure-flow network, the equipment items were sized, and then the lower level control system was implemented in Aspen Plus Dynamics. The Aspen Plus flowsheet of the CO₂ compression system is shown in Figure 2-3.

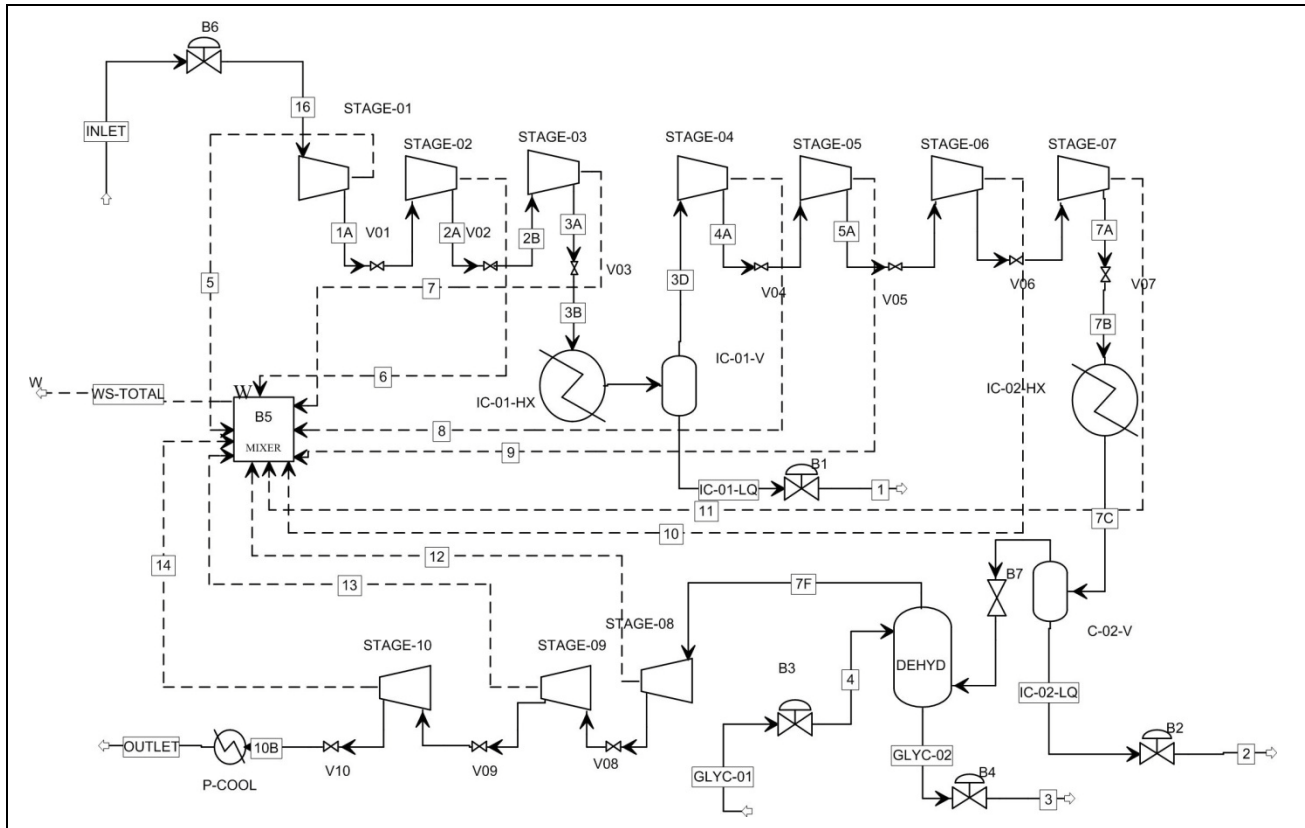


Figure 2-3 Aspen Plus flowsheet of the CO₂ compression system

A 10-stage inline centrifugal compressor is used for compressing CO₂ from 22 psia to 2,200 psia. According to the steady-state model obtained from Task Set 3, the water content of the CO₂ stream entering the compressor is approximately 3.5 wt% (8 vol%) and the remainder (92 vol%) is CO₂. The compressor can be divided into three sections – low pressure (LP), medium pressure (MP), and high pressure (HP). The LP section uses three stages to compress the CO₂-rich stream to about 96.5 psia. After cooling the stream in a water-cooler (IC-01-HX) and separating the free water in a flash-vessel (IC-01-V), the CO₂-rich stream is sent to the MP section where it is

compressed to 614.8 psia in four stages. The stream is then cooled (IC-02-HX) and water is separated in a flash vessel (IC-02-V) before sending it to a glycol tower (DEHYD) for further removal of water. The CO₂-rich stream from the top of the glycol tower is sent to the HP section where it is compressed in three stages. The compressed stream with a CO₂ concentration of 99.8 mol% is cooled (P-COOL) before sending it to the pipeline.

The Peng-Robinson equation of state with the Boston-Mathias modifications was used to calculate stream properties, and the isentropic ASME method was used for compressor calculations. The water-coolers are exported with “LMTD” option to Aspen Plus Dynamics. In this option, the effect of the flowrate of the medium and its temperature change due to heat exchange are considered. Counter-current configuration with a medium inlet temperature of 29.5°C was considered. During dynamic simulation, the cooling water flowrate is left unchanged. The material of construction for the flash vessels and the coolers are considered to be carbon-steel. PID controllers are used in designing the lower-level control system. The CO₂ compression process remains stable in face of the disturbances as seen from the results in the following section.

3.0 Results and Discussion

3.1 Flow-driven dynamic simulation of the solid-sorbent adsorber

Transient simulations have been performed with both single-stage adsorbers (under-flow and over-flow) and a two-stage adsorber. The disturbances considered in the following studies are the ones expected during transient operation of a supercritical PC plant due to changes in the plant throughput, CO₂ capture rates, changes in the coal composition, and changes in the plant operating conditions. It is important to note that the dynamic results reported below are for open-loop simulations.

3.1.1 Single stage adsorber – Overflow type

Case I: A Step change in the flue gas flow rate

The flue gas flowrate is step increased by 20 kmol/hr (from 10,500 to 10,520 kmol/hr) at 2 sec. The dynamics of the exit bubble phase temperature, emulsion phase solids temperature, and CO₂ concentration at the gas exit are shown in Figures 3-1, 3-2, and 3-3, respectively. As expected, the temperature of the bubble (gas) phase decreases with increase in the flue gas flowrate since the gas spends less time in the adsorber before exiting. As a result, the sensitive heat transfer from the gas phase to the solid phase increases and hence the solids temperature rises. The concentration of CO₂ in the leaving gas stream increases due to lesser residence time of the flue gas in the bed; that is, less CO₂ is captured in the bed.

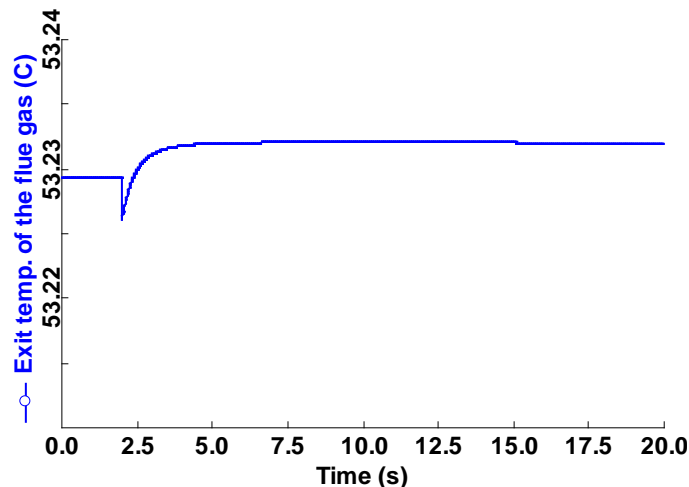


Figure 3-1 Dynamics of the bubble phase temperature at the exit of the adsorber due to 20 kmol/hr step increase in the flue gas flow rate

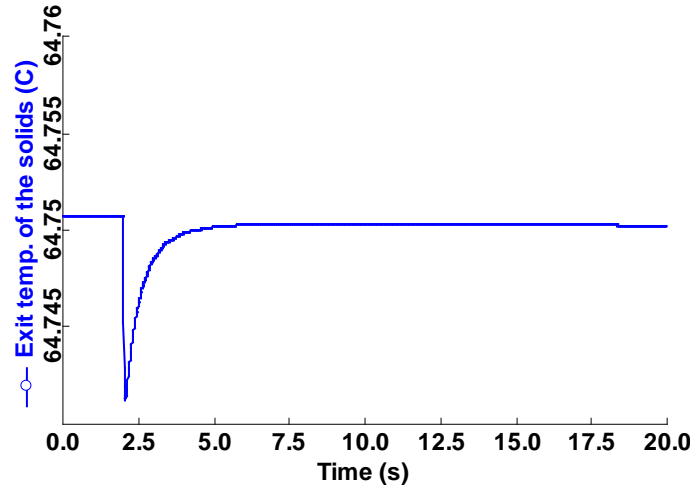


Figure 3-2 Dynamics of the emulsion phase solids temperature at the exit of the adsorber due to 20 kmol/hr step increase in the flue gas flow rate

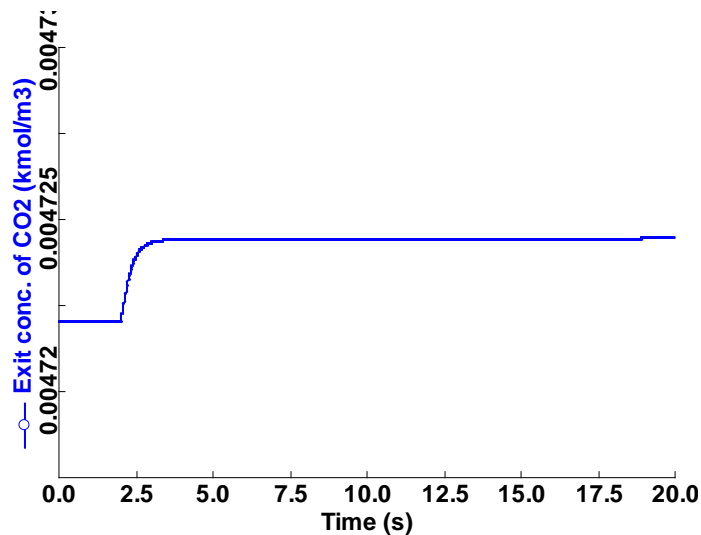


Figure 3-3 Dynamics of the CO₂ concentration at the exit of the adsorber due to 20 kmol/hr step increase in the flue gas flow rate

Case II. Step change in the solids inlet temperature

The solids inlet temperature is step increased by 4°C (from 90°C to 94°C) at 2 sec. The dynamics of the exit bubble phase temperature, emulsion phase solids temperature, and CO₂ concentration at the gas exit are shown in Figures 3-4, 3-5, and 3-6, respectively. As expected, the temperatures of the gases and solid increases in the bed and also at the exit. Since CO₂ adsorption reaction is exothermic and equilibrium-limited, the extent of reaction decreases with the increase in

temperature of the solids in the bed. Hence, less CO₂ is captured and the concentration of CO₂ in the flue gas at the exit increases.

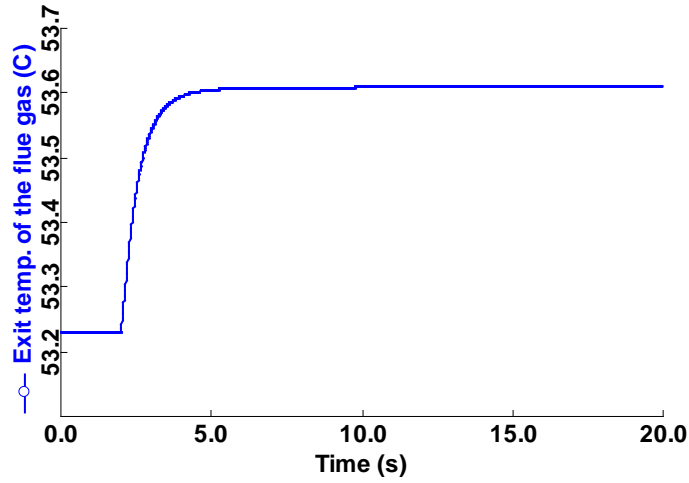


Figure 3-4 Dynamics of the bubble phase temperature at the exit of the adsorber as a result of 4°C step increase in the solids inlet temperature

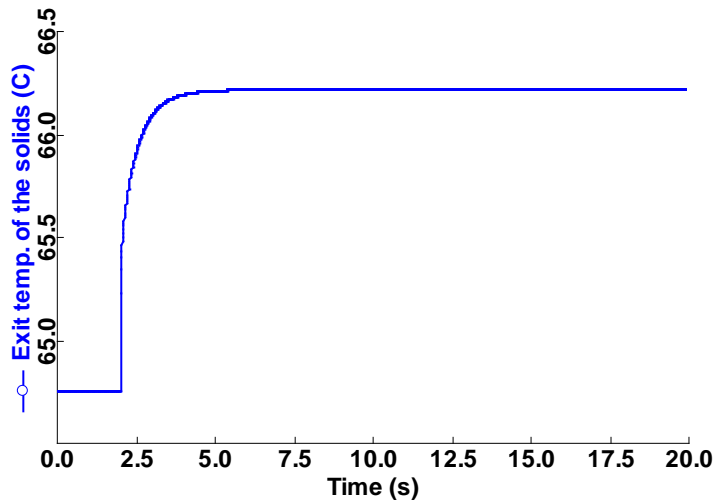


Figure 3-5 Dynamics of the emulsion phase solids temperature at the exit of the adsorber as a result of 4° C step increase in the solids inlet temperature

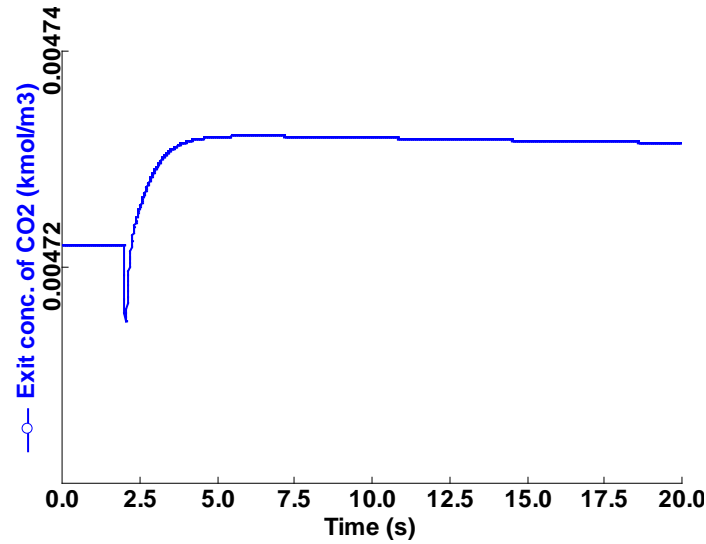


Figure 3-6 Dynamics of the CO₂ concentration at the exit of the adsorber as a result of 4° C step increase in the solids inlet temperature

Case III: Step change in the solids flow rate

The solids flowrate is step increased by 5% (from 420.83 kg/s to 441.875 kg/s) at 2 sec. As a result, a decrease in the temperature of emulsion phase solids is observed since the solids spend less time in the adsorber. The dynamics of the exit bubble phase temperature, emulsion phase solids temperature, and CO₂ concentration in the gas exit are shown in Figures 3-7, 3-8, and 3-9, respectively. As expected, the extent of adsorption increases and hence the concentration of CO₂ at the flue gas exit decreases.

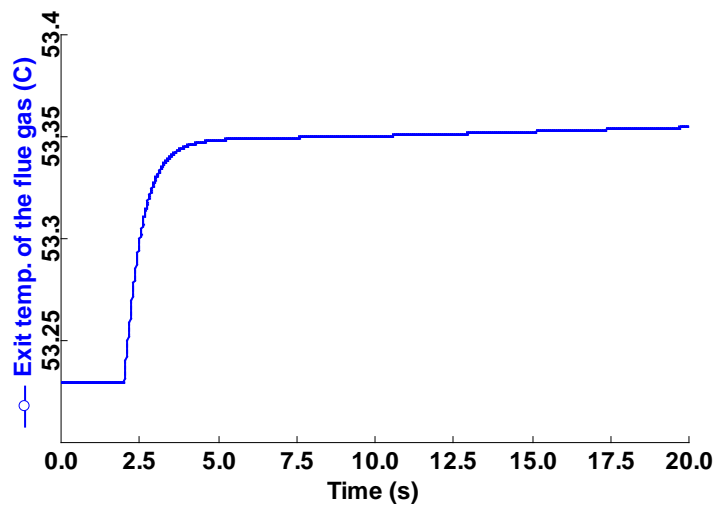


Figure 3-7 Dynamics of the bubble phase temperature at the exit of the adsorber as a result of 5% step increase in the solids flow rate

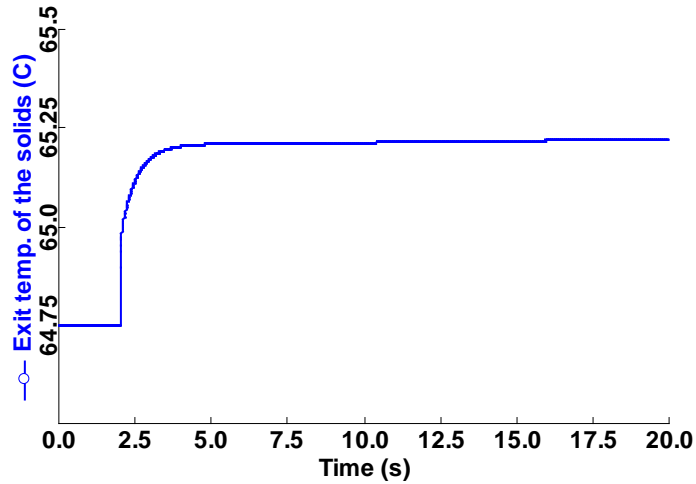


Figure 3-8 Dynamics of the emulsion phase solids temperature at the exit of the adsorber as a result of 5% step increase in the solids flow rate

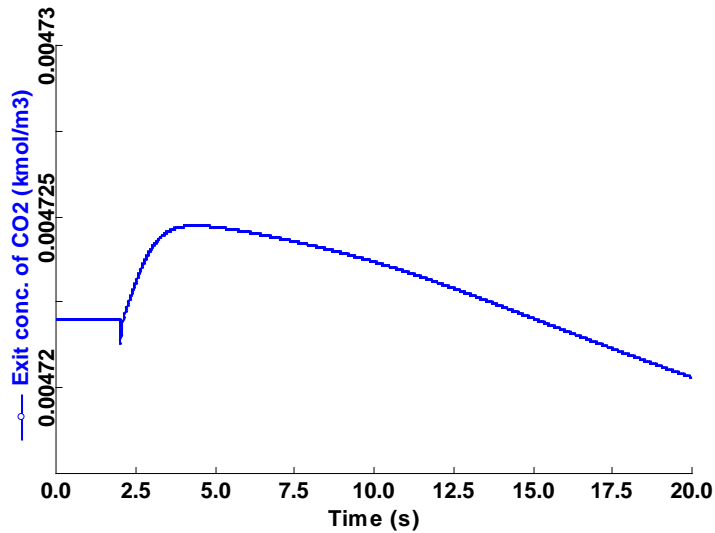


Figure 3-9 Dynamics of the CO₂ concentration at the exit of the adsorber as a result of 5% step increase in the solids flow rate

Case IV: Step change in the flue gas inlet composition

The mole fraction of CO₂ in the inlet flue gas stream is step increased by 10% (from 0.1 to 0.11) at 2 sec. The dynamics of the exit bubble phase temperature, emulsion phase solids temperature, and CO₂ concentration in the gas exit are shown in Figures 3-10, 3-11, and 3-12, respectively. Due to increase in partial pressure of CO₂ in the flue gas, the quantity of the CO₂ adsorbed increases. As a result, exit bubble phase temperature and emulsion phase solids temperature increases. Figure 3-12 shows that this step results in a higher CO₂ concentration in the fluegas at the adsorber outlet.

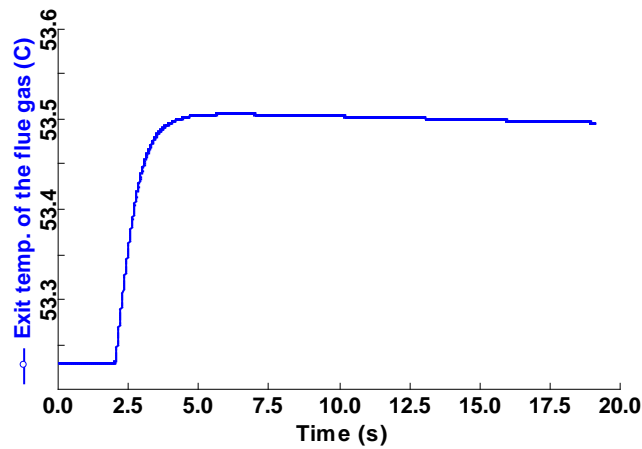


Figure 3-10 Dynamics of the bubble phase temperature at the exit of the adsorber due to 10% step increase in the CO₂ mole fraction in the flue gas inlet stream

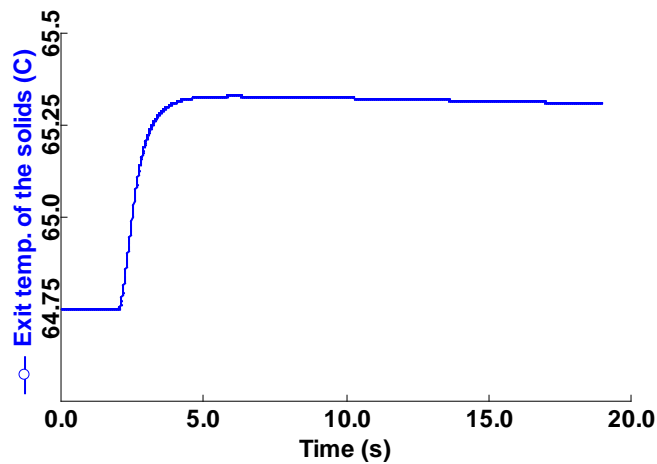


Figure 3-11 Dynamics of the emulsion phase solids temperature at the exit of the adsorber due to 10% step increase in the CO₂ mole fraction in the flue gas inlet stream

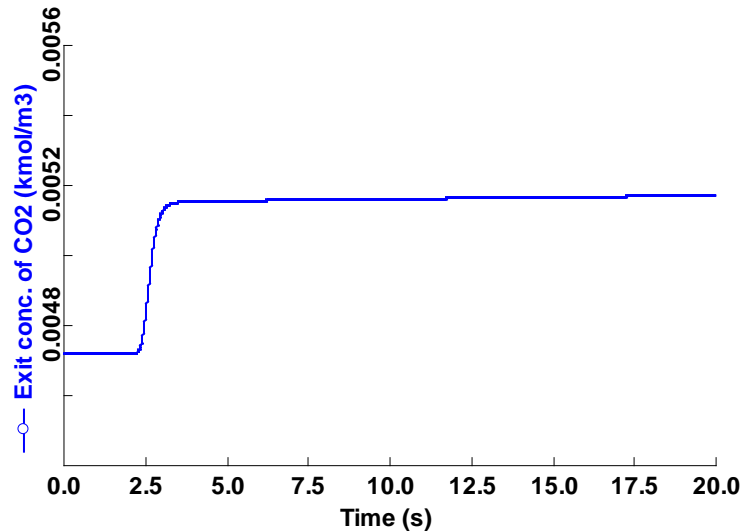


Figure 3-12 Dynamics of the CO₂ concentration at the exit of the adsorber due to 10% step increase in the CO₂ mole fraction in the flue gas inlet stream

3.1.2 Single-stage adsorber – Underflow-type

Step disturbances similar to before are introduced to the single-stage adsorber with underflow-type configuration and the key differences are observed.

Case I: A Step change in the flue gas flow rate

The transient responses of gas and solids temperatures and CO₂ concentration at the exit of the adsorber are shown in Figures 3-13, 3-14, and 3-15, respectively for a step change in the inlet flue gas flowrate. Compared to the overflow configuration, the settling time for the solids exit temperature is more in this case since the distance between the location of the entry and exit locations of the solids is greater in the underflow-type configuration.

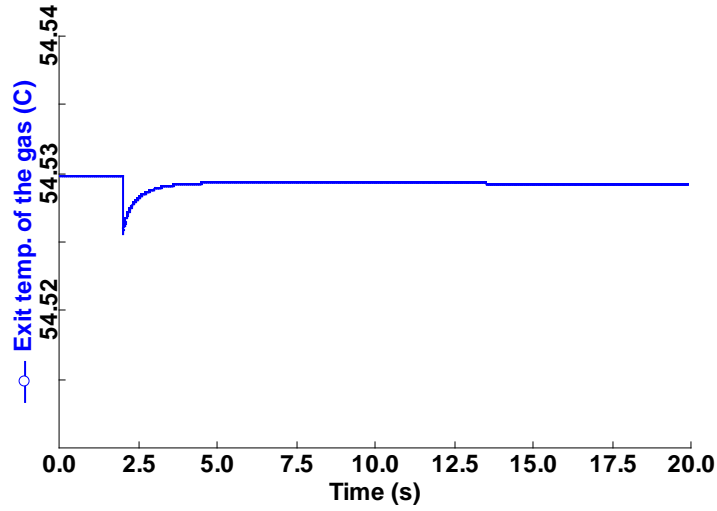


Figure 3-13 Dynamics of the bubble phase temperature at the exit of the adsorber due to 20 kmol/hr step increase in the flue gas flow rate

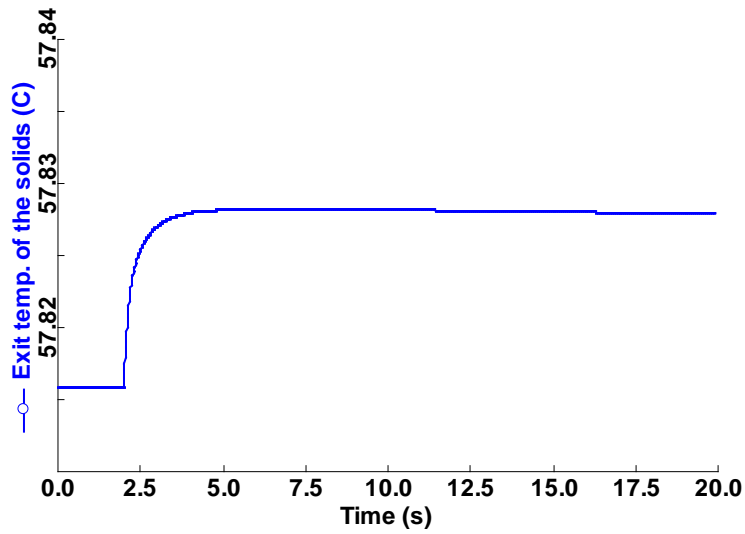


Figure 3-14 Dynamics of the emulsion phase solids temperature at the exit of the adsorber due to 20 kmol/hr step increase in the flue gas flow rate

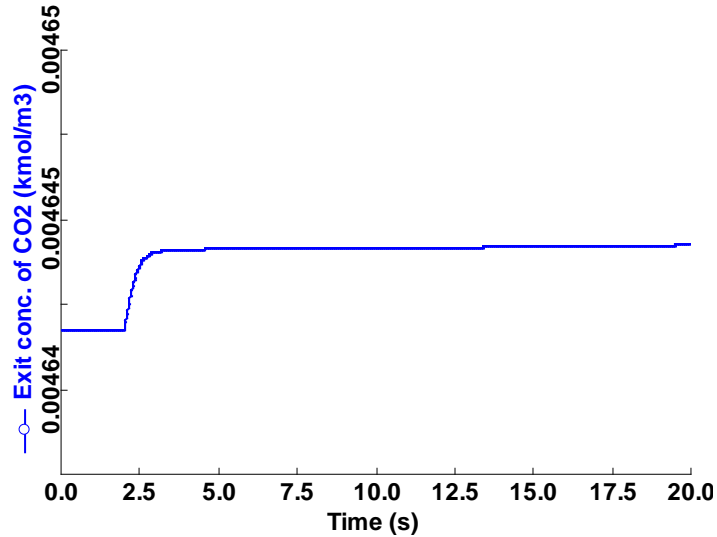


Figure 3-15 Dynamics of the CO₂ concentration at the exit of the adsorber due to 20 kmol/hr step increase in the flue gas flow rate

Case II. Step change in the solids inlet temperature

The dynamics of exit temperature of gas and solids and concentration of CO₂ at the gas exit are shown in Figures 3-16, 3-17, and 3-18, respectively for a step change in the solids inlet temperature. Because of proximity of the entry and exit locations of the solids in the overflow-type configuration, the exit temperature of the solids increases more in the overflow-type configuration for a step change of same magnitude in the inlet temperature. The decrease in the extent of adsorption is more in the underflow-type configuration resulting in a higher change of CO₂ concentration in the flue gas at the outlet.

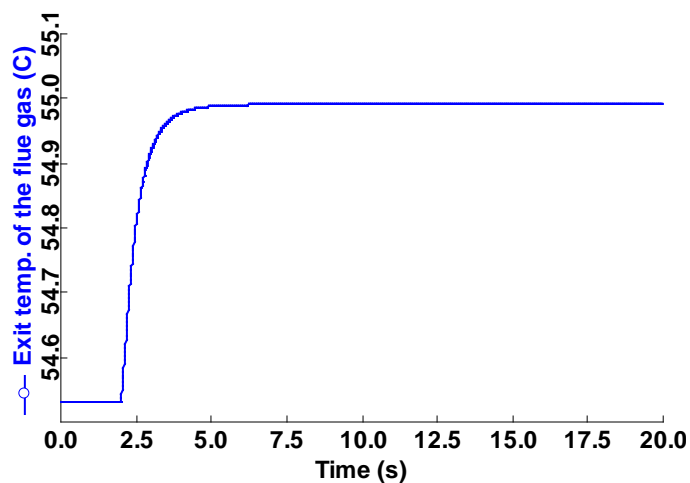


Figure 3-16 Dynamics of the bubble phase temperature at the exit of the adsorber as a result of 4°C step increase in the solids inlet temperature

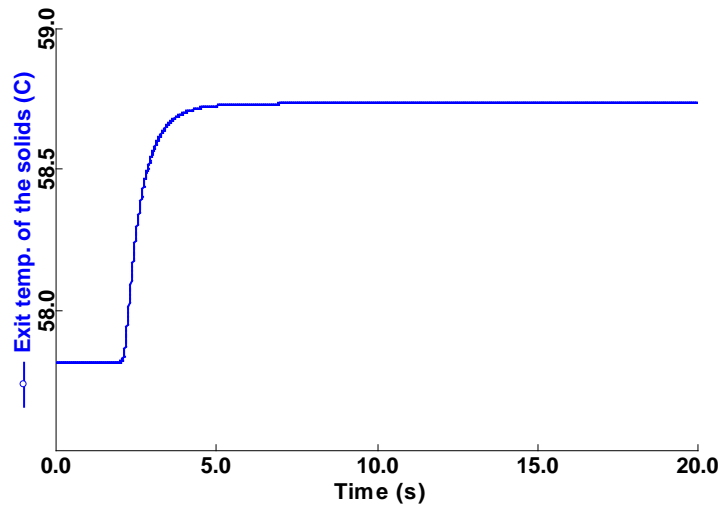


Figure 3-17 Dynamics of the emulsion phase solids temperature at the exit of the adsorber as a result of 4°C step increase in the solids inlet temperature

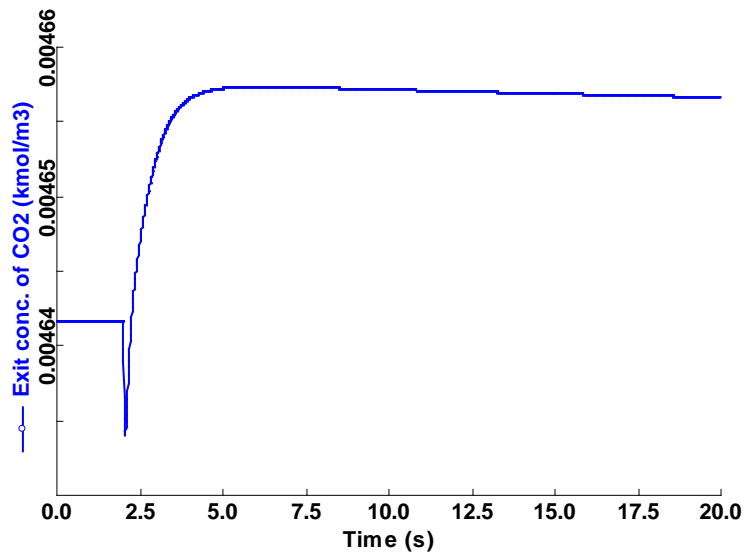


Figure 3-18 Dynamics of the CO₂ concentration at the exit of the adsorber as a result of 4°C step increase in the solids inlet temperature

Case III: Step change in the solids flow rate

Similar to temperature, a step change of the same magnitude in the solids inlet flow rate has more impact in the overflow-type configuration. The transient responses for a step change in the solids inlet flow rate are shown in Figures 3-19 to 3-21.

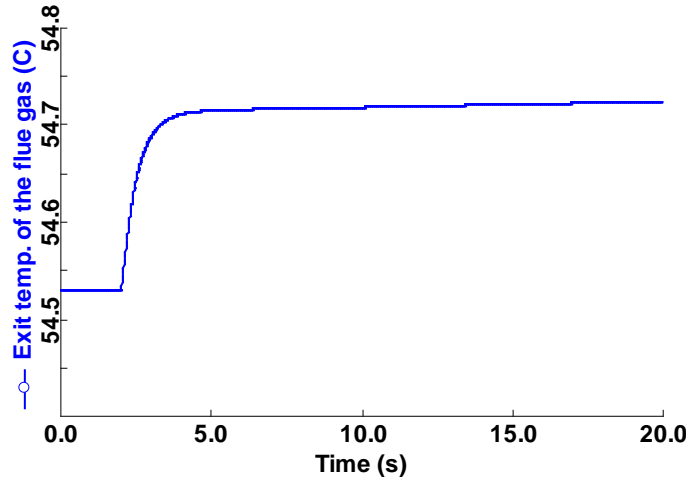


Figure 3-19 Dynamics of the bubble phase temperature at the exit of the adsorber as a result of 5% step increase in the solids flow rate

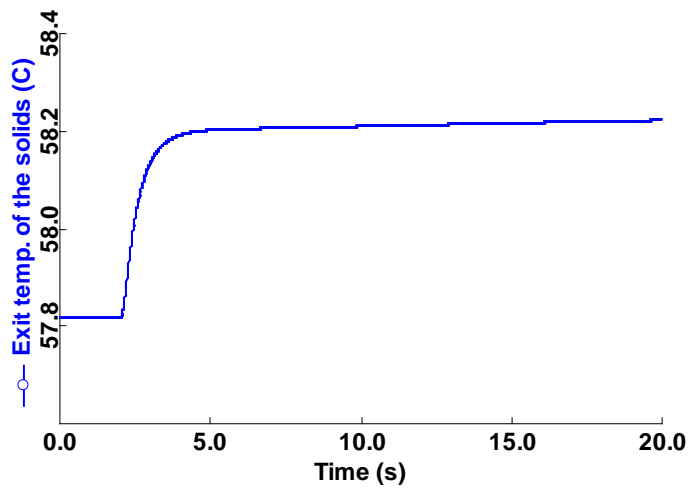


Figure 3-20 Dynamics of the emulsion phase solids temperature at the exit of the adsorber as a result of 5% step increase in the solids flow rate

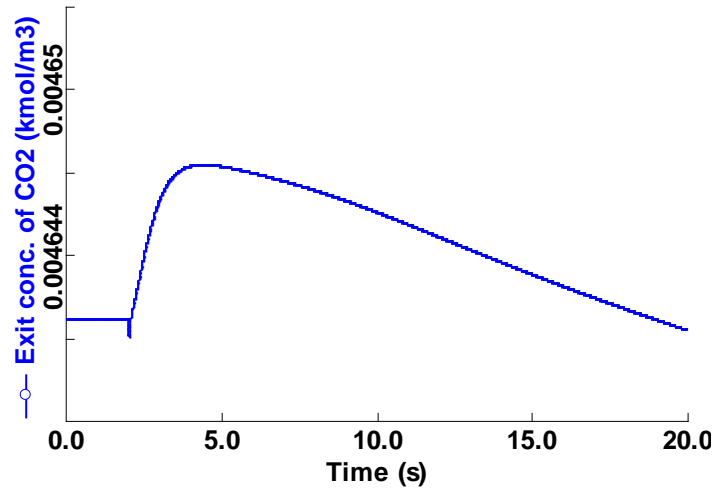


Figure 3-21 Dynamics of the CO₂ concentration at the exit of the adsorber as a result of 5% step increase in the solids flow rate

Case IV: Step change in the flue gas inlet composition

As the mole fraction of CO₂ in the inlet flue gas stream is step increased by 10% (from 0.1 to 0.11) at 2 sec, the rate of adsorption increases. The transient responses are shown in Figure 3-22 to 3-24. The settling time and the extent of adsorption is more in the underflow-type configuration because of the greater distance between the inlet and outlet locations. Hence, the concentration of CO₂ at the exit is lesser for the underflow-type configuration.

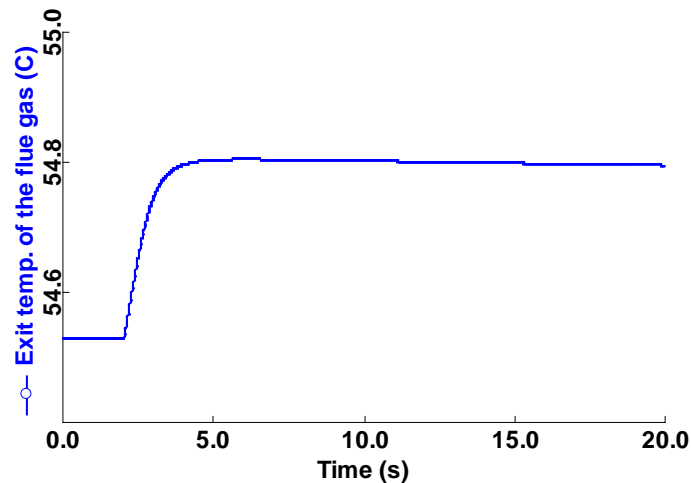


Figure 3-22 Dynamics of the bubble phase temperature at the exit of the adsorber as a result of 10% step increase in the CO₂ mole fraction in the flue gas inlet stream

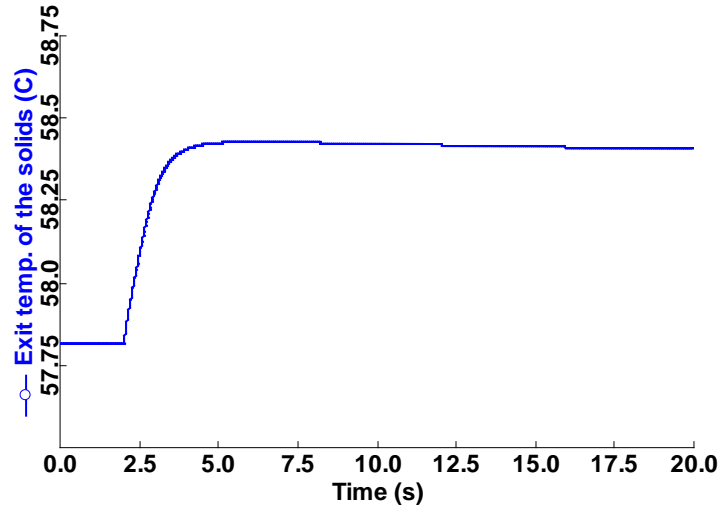


Figure 3-23 Dynamics of the emulsion phase solids temperature at the exit of the adsorber as a result of 10% step increase in the CO₂ mole fraction in the flue gas inlet stream

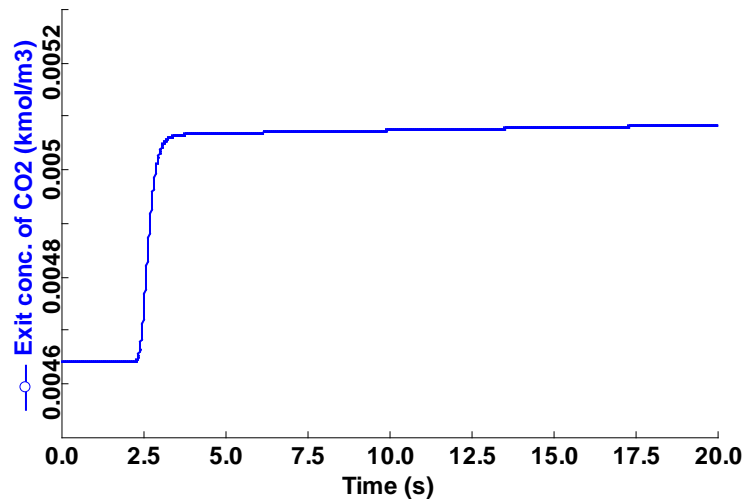


Figure 3-24 Dynamics of the CO₂ concentration at the exit of the adsorber as a result of 10% step increase in the CO₂ mole fraction in the flue gas inlet stream

3.1.3 Two- stage adsorber

Similar to the single-stage adsorber, the dynamics of the bubble phase gas and emulsion phase solids exit temperatures have been studied along with the exit concentration of CO₂ in the flue gas. In the following plots, Stage 1 represents the lower adsorber (where flue gas enters) and

Stage 2 represents the upper or second stage adsorber (where fresh sorbent is loaded). From operational point of view, underflow-type configuration has been considered for the first adsorber (Stage 1) and overflow-type configuration has been considered for the second bed (Stage 2) in the following dynamic simulations.

Case I: A step change of 5% in the solids flow rate introduced at 2 sec.

A step change of 5% (from 166.67 kg/s to 175 kg/s) is introduced in the solids inlet flow rate. As described earlier, fresh solids (sorbent) enters at Stage 2. The increase in the solids flow enhances the extent of adsorption in both the stages. As a result, a lower concentration of CO₂ is achieved at the exit flue gas.

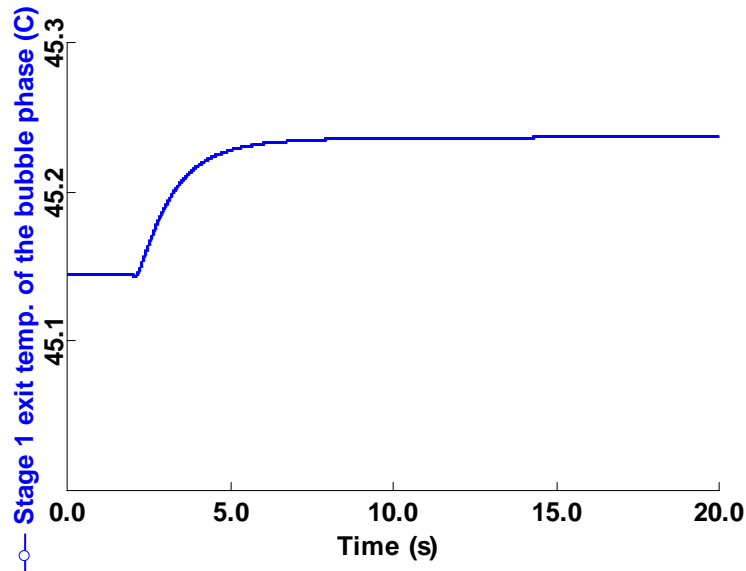


Figure 3-25. Dynamics of the bubble phase temperature at the exit of Stage 1 as a result of 5% step increase in the solids flow rate

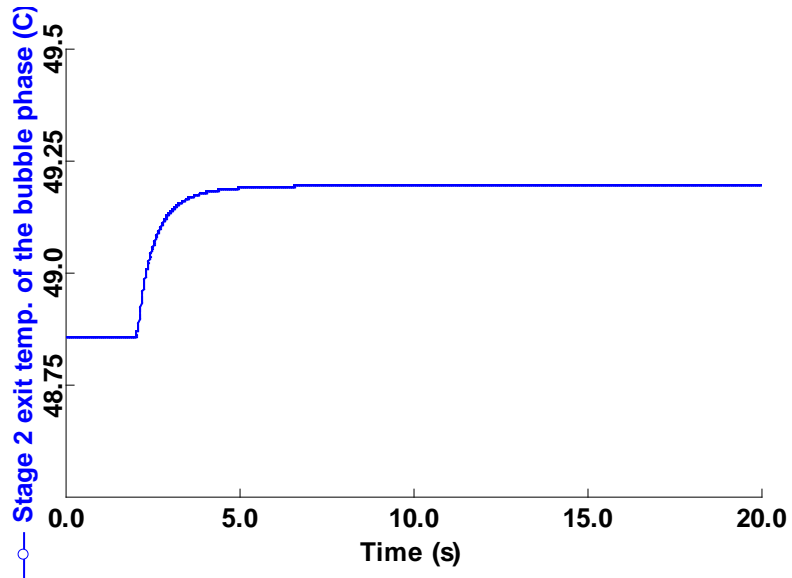


Figure 3-26 Dynamics of the bubble phase temperature at the exit of Stage 2 as a result of 5% step increase in the solids flow rate

The transient responses of the solids exit temperatures from Stage 1 and Stage 2 are shown in Figures 3-27, and 3-28, respectively. Since fresh sorbent enters at Stage 2, the rate of adsorption is more in this stage. As a result, the change in the solids exit temperature is more in Stage 2 compared to Stage 1.

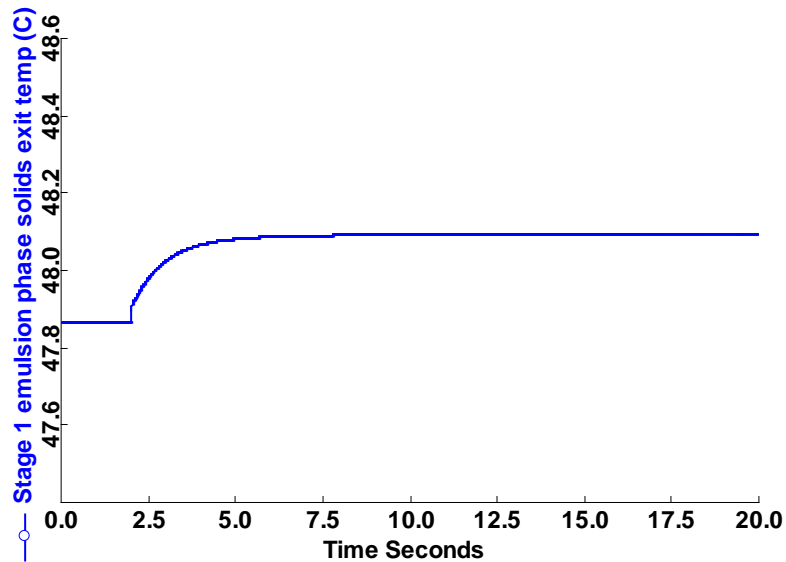


Figure 3-27. Dynamics of the emulsion phase solids temperature at the exit of stage 1 as a result of 5% step increase in the solids flow rate

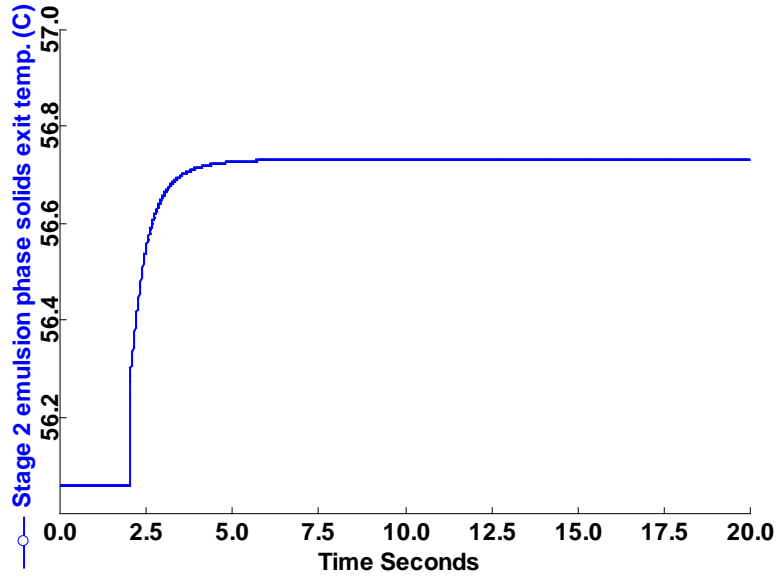


Figure 3-28. Dynamics of the emulsion phase solids temperature at the exit of Stage 2 as a result of 5% step increase in the solids flow rate

As the solids are introduced at Stage 2 and the extent of adsorption is more in Stage 2, a step change in the solids flowrate causes an initial rapid change in the CO₂ concentration from Stage 2 whereas the change in the CO₂ concentration from Stage 1 is gradual. This in turn affects the dynamics of Stage 2. The dynamics of CO₂ concentration at the exit of Stage 1 and Stage 2 are shown in Figures 3-29 and 3-30, respectively.

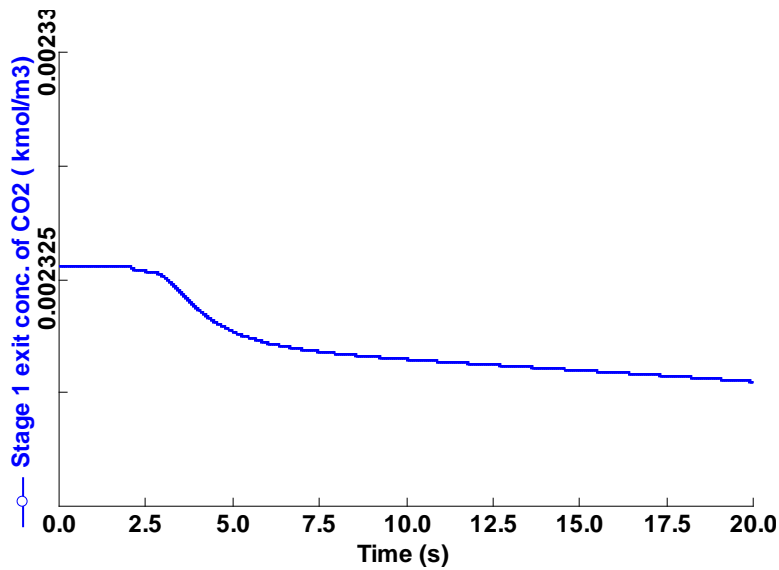


Figure 3-29. Dynamics of the concentration of CO₂ at the exit of Stage 1 as a result of 5% step increase in the solids flow rate

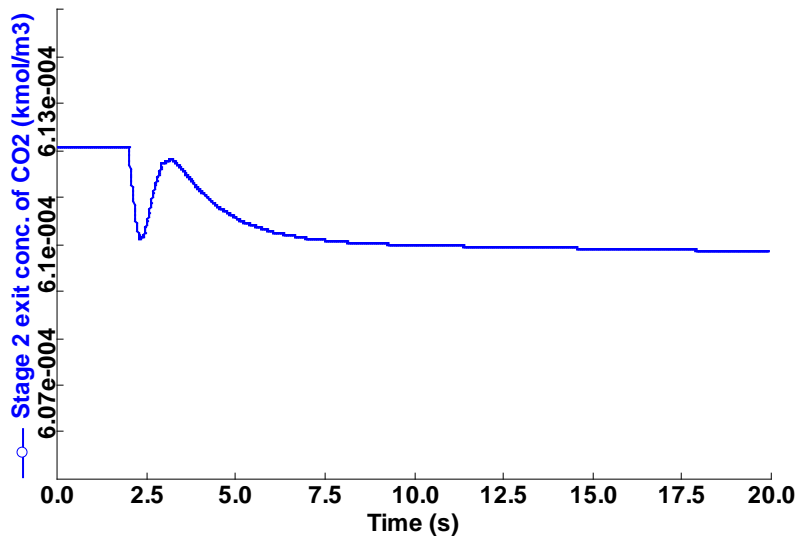


Figure 3-30. Dynamics of the concentration of CO₂ at the exit of Stage 2 as a result of 5% step increase in the solids flow rate

Case II: A step increase of 4°C in the solids inlet temperature introduced at 2 sec

In this study, a step increase of 4°C (from 122°C to 126°C) is introduced in the solids inlet temperature. As mentioned earlier, change in the solids conditions has relatively more effect on the Stage 2 conditions than on Stage 1. This is reflected in the transients of the flue gas exit temperature shown in Figures 3-31 and 3-32 for Stage 1 and Stage 2, respectively.

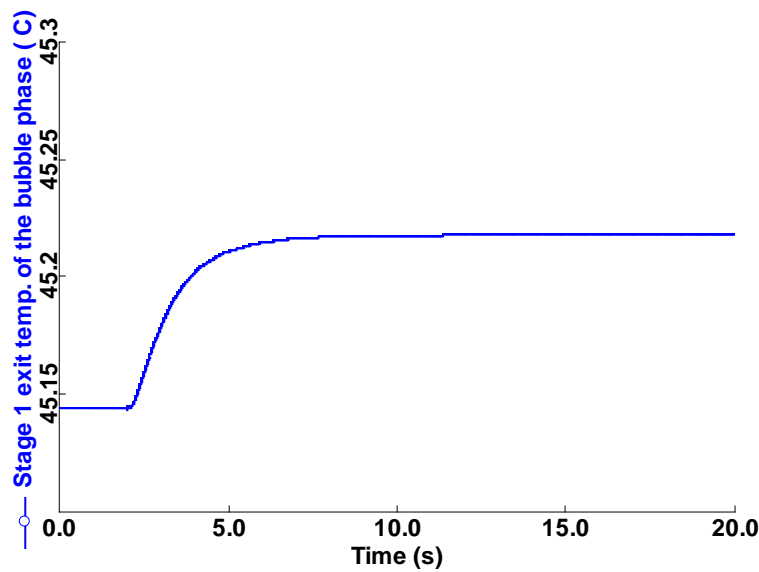


Figure 3-31. Dynamics of the bubble phase temperature at the exit of the Stage 1 as a result of 4°C step increase in the solids inlet temperature

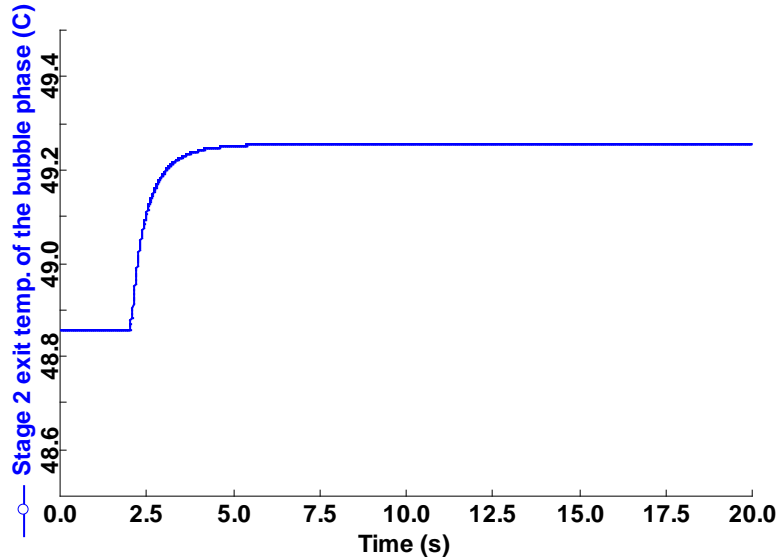


Figure 3-32. Dynamics of the bubble phase temperature at the exit of Stage 2 as a result of 4°C step increase in the solids inlet temperature

The dynamics of solids exit temperature from Stage 1 and Stage 2 are shown in Figures 3-33 and 3-34, respectively. A sharper increase in the exit temperature is observed in Stage 2.

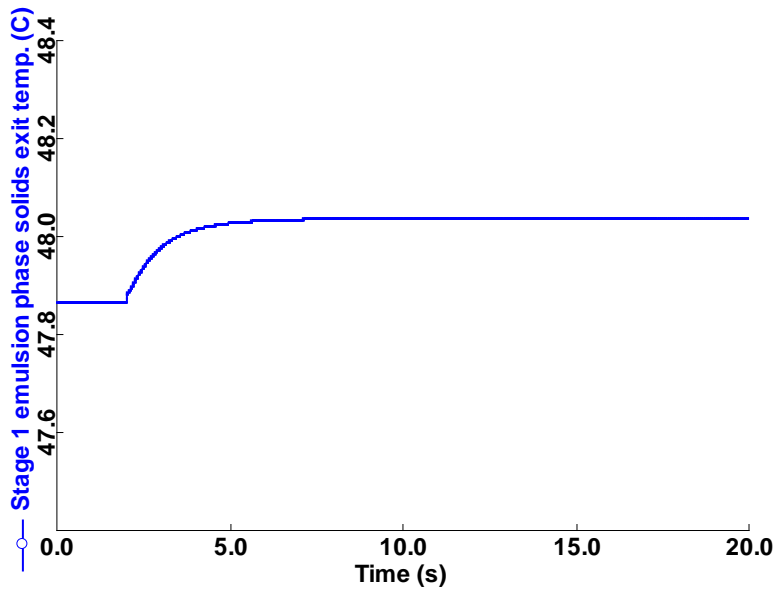


Figure 3-33. Dynamics of the emulsion phase solids temperature at the exit of the stage 1 as a result of 4°C step increase in the solids inlet temperature

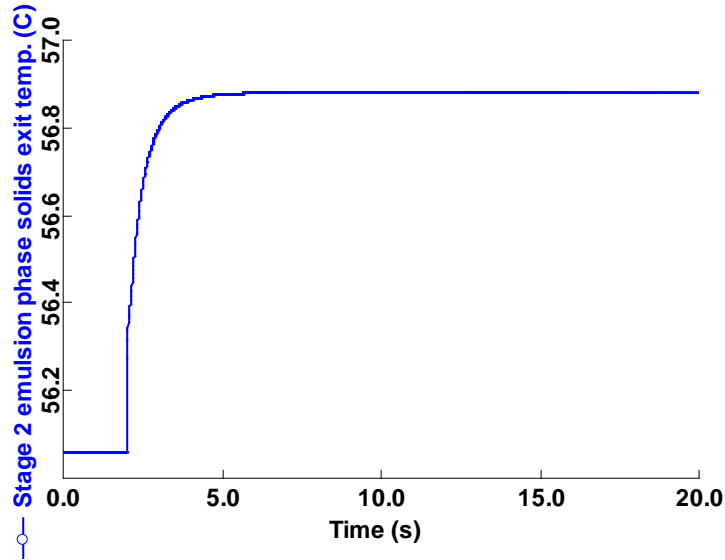


Figure 3-34. Dynamics of the emulsion phase solids temperature at the exit of the stage 2 as a result of 4°C step increase in the solids inlet temperature

Similar to the responses shown before, the change in the exit concentration of CO₂ from Stage 1 is gradual compared to that from Stage 2 as shown in Figure 3-35, and Figure 3-36, respectively.

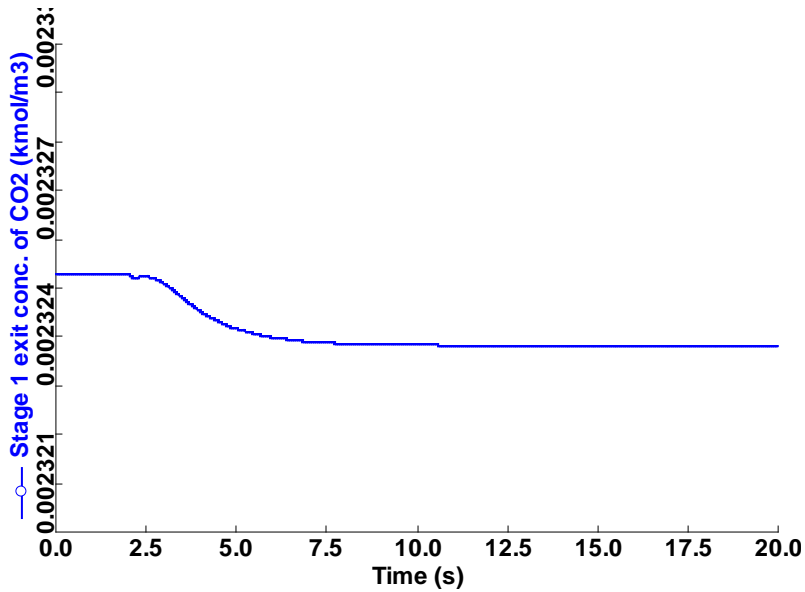


Figure 3-35. Dynamics of the concentration of CO₂ at the exit of Stage 1 as a result of 4°C step increase in the solids inlet temperature

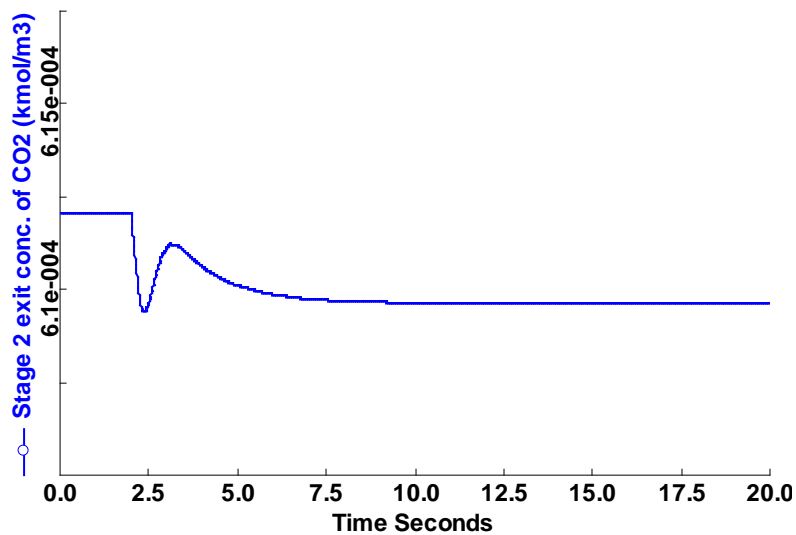


Figure 3-36. Dynamics of the concentration of CO₂ at the exit of Stage 2 as a result of 4°C step increase in the solids inlet temperature

3.2 Pressure-driven dynamic simulation of the CO₂ compression system

Default performance curves available in Aspen Plus Dynamics for compressors are used for the following dynamic simulations. The mechanical and isentropic efficiencies of the compressor modules remain fixed at their respective steady state values.

3.2.1 Increase in the CO₂ flowrate

In the operation of a supercritical PC plant, CO₂ flowrate to the compression system can vary because of a change in the plant throughput, and/or higher CO₂ capture, and/or higher carbon content of the coal at a given throughput. The lower level control system of the CO₂ compression should be designed to reject this disturbance. To simulate this disturbance, the inlet pressure of the CO₂-rich stream to the compression system is step increased as shown in Figure 3-37.

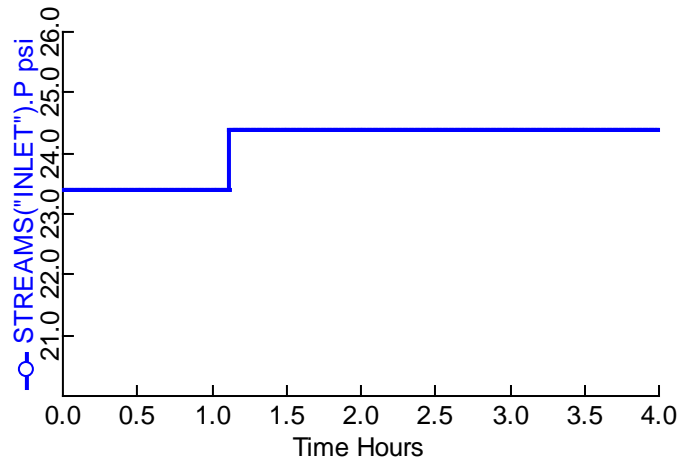


Figure 3-37 Step change in the inlet pressure of the CO₂-rich stream

As a result, the flowrate of the inlet-stream increases reaching its new steady-state value very quickly as shown in Figure 3-38.

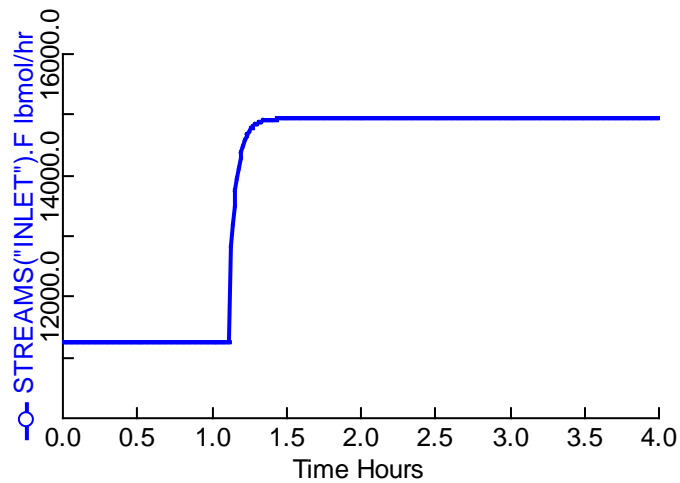


Figure 3-38 Transients in the inlet flowrate due to step change in the inlet pressure

Due to the change in the flowrate, the outlet pressure of the LP, MP, and HP sections increases initially. However as the compressor power is increased, these pressures return back to their previous values. The transients in the outlet pressure of the LP section, MP section, and the

discharge of the second stage in the HP section are shown in Figure 3-39, 3-40, and 3-41, respectively.

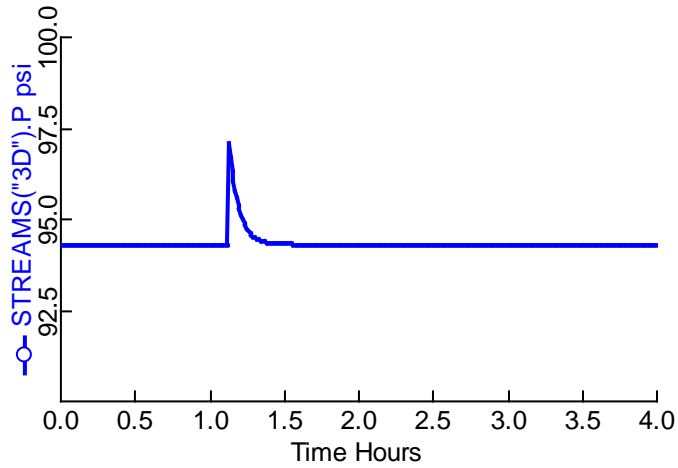


Figure 3-39 Transients in the outlet pressure of the LP section due to step increase in the inlet pressure

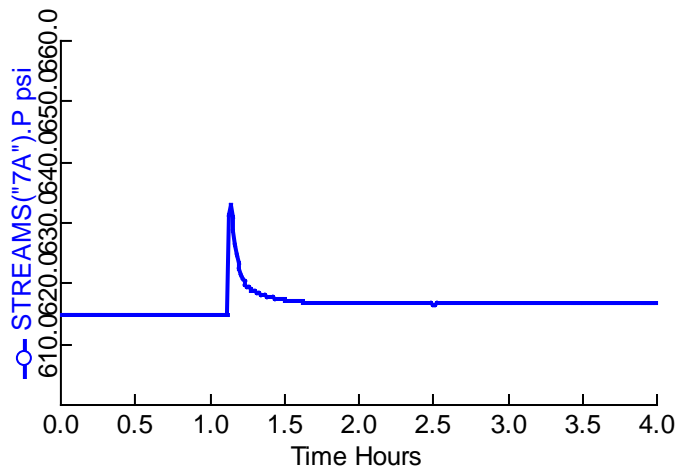


Figure 3-40 Transients in the outlet pressure of the MP section due to step increase in the inlet pressure

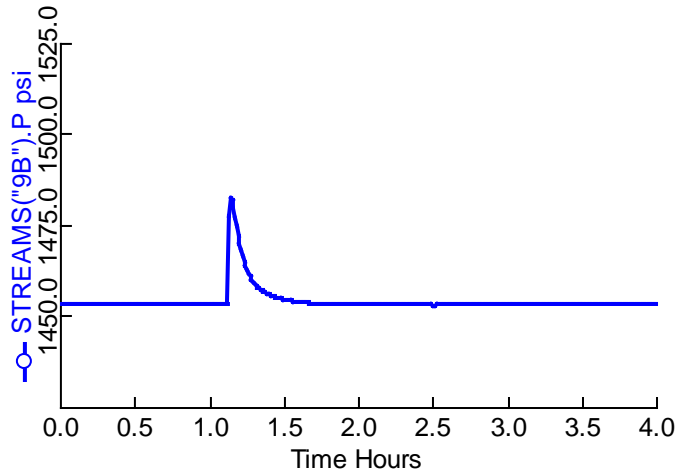


Figure 3-41 Transients in the discharge of the second stage in the HP section due to step increase in the inlet pressure

As expected, the change in the overall flowrate results in an overall increase in the compression power as shown in Figure 3-42. Even though the differences are minor, the LP section has the least settling time followed by the MP and the HP section, respectively. The settling time for the transients in the power consumption is the same as the transients of the HP section.

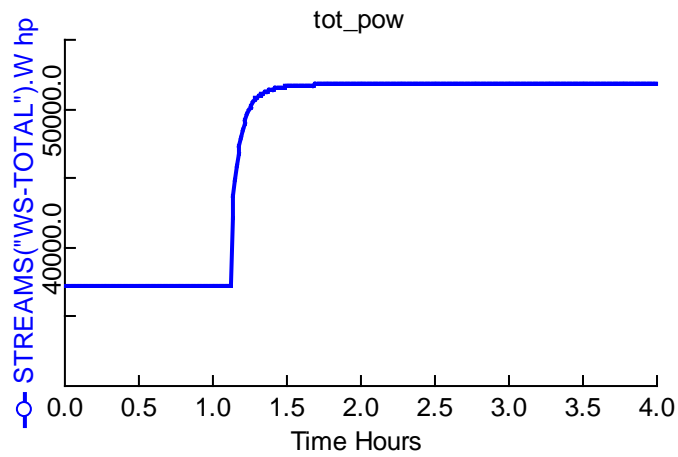


Figure 3-42 Increase in the total power requirement due to step increase in the inlet pressure

3.2.2 Decrease in the CO₂ flowrate

Similar to before, for simulating the disturbance due to decrease in the CO₂ flowrate, the inlet pressure of the CO₂-rich stream to the compression system is step decreased as shown in Figure 3-43.

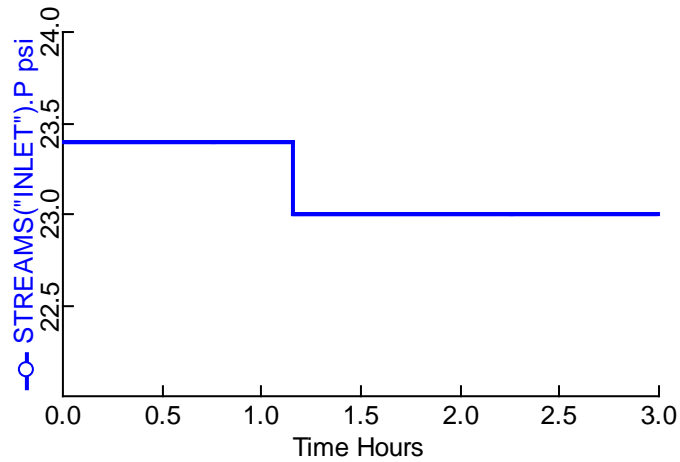


Figure 3-43 Step decrease in the inlet pressure of the CO₂-rich stream

As a result, the flowrate of the inlet-stream decreases reaching its new steadystate value very quickly as shown in Figure 3-44.

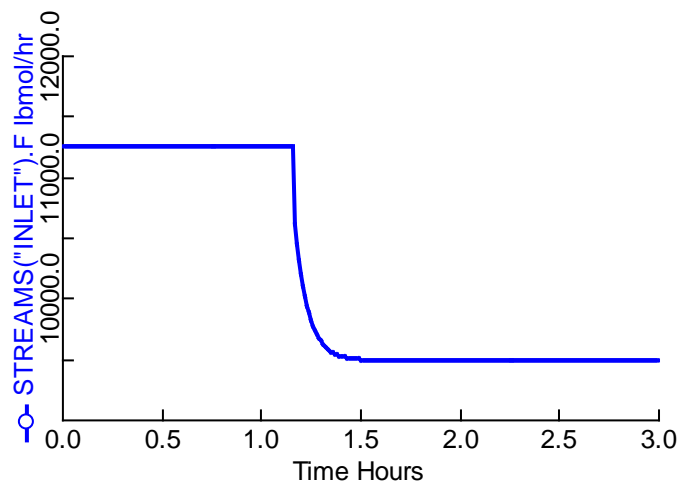


Figure 3-44 Transients in the inlet flowrate due to step decrease in the inlet pressure

Due to the decrease in the flowrate, the outlet pressures of the LP, MP, and HP sections decrease initially. However as the compressor power is decreased, these pressures returns back to their previous values. The transients in the outlet pressure of the LP section, MP section, and the discharge of the second stage in the HP section are shown in Figure 3-45, 3-46, and 3-47, respectively.

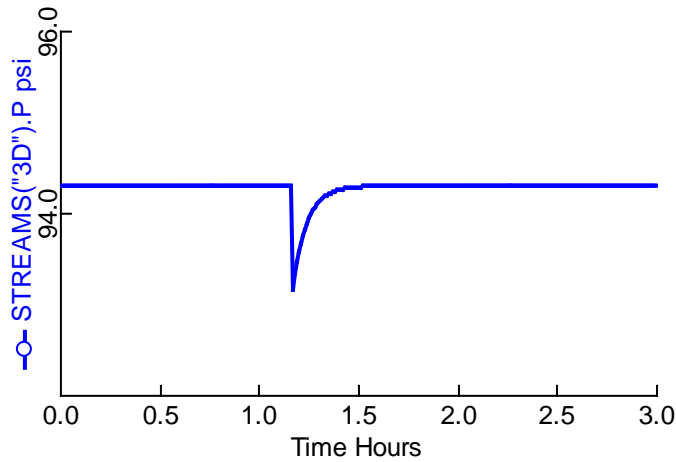


Figure 3-45 Transients in the outlet pressure of the LP section due to step decrease in the inlet pressure

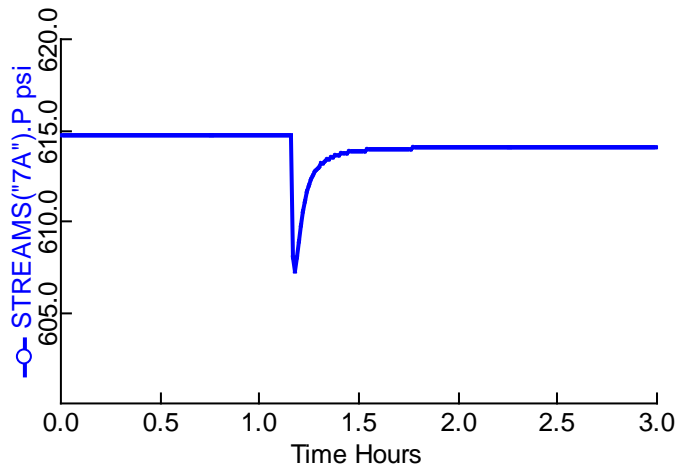


Figure 3-46 Transients in the outlet pressure of the MP section due to step decrease in the inlet pressure

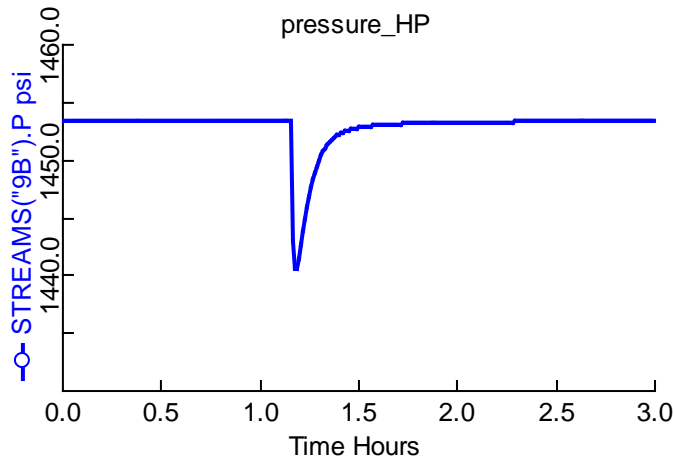


Figure 3-47 Transients in the discharge of the second stage in the HP section due to step decrease in the inlet pressure

As expected, the change in the overall flowrate results in an overall decrease in the compression power as shown in Figure 3-48. Even though the differences are minor, the LP section has the least settling time followed by the MP and the HP section, respectively. The settling time for the transients in the power consumption is the same as the transients of the HP section.

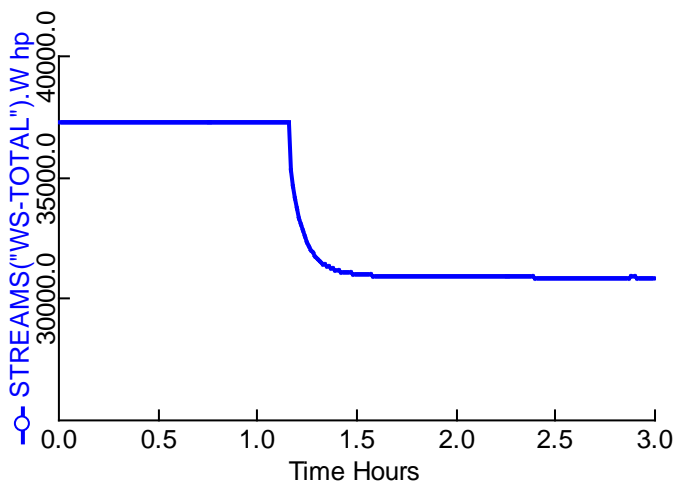


Figure 3-48 Decrease in the total power requirement due to step decrease in the inlet pressure

3.2.2 Decrease in the CO₂ concentration

Concentration of CO₂ in the stream to the compression system can vary due to operational changes in the CO₂ capture system. Even though, the sequestration stream is desired to be very pure (>99%), the concentration may vary at times and thus, the lower level control system in the CO₂ compression process should be designed to reject this disturbance. To simulate this disturbance, the CO₂ concentration of the inlet stream is step decreased from 92 mol% to 85 mol% as shown in Figure 3-49. N₂ concentration which is 0 mol% at steady-state is step increased to 7 mol% simultaneously.

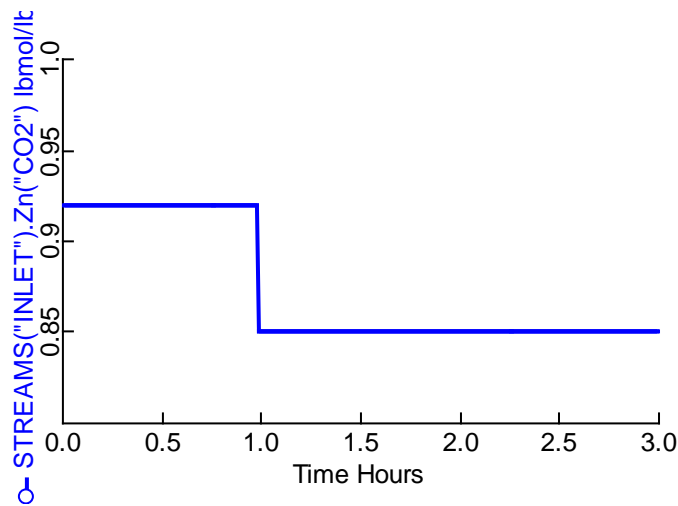


Figure 3-49 Step decrease in the CO₂ concentration at the inlet

As the density of the inlet feed decreases (from 0.156 lb/ft³ to 0.152 lb/ft³) due to this change, the inlet flowrate increases for a given inlet pressure. To simulate the effect of the change in the concentration when the molar flowrate of the feed remains unchanged a controller is installed at the inlet that maintains the inlet flowrate. The transient response of the flowrate is shown in Figure 3-50. A small increase in the flowrate is observed initially, quickly returning to its previous value as the inlet control valve is manipulated.

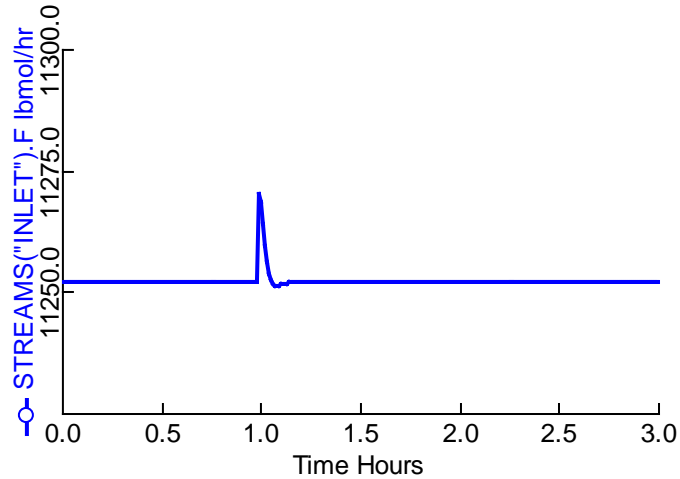


Figure 3-50 Transients in the inlet flowrate

Due to the initial increases in the flowrate, the outlet pressure of the LP section, MP section, and the discharge of the second stage in the HP section increases initially as seen in Figures 3-51, 3-52, and 3-53, respectively. Similar trends have been observed before due to the increase in the flowrate. As the flowrate returns to its previous value, the pressures reach their new steady-state values. There is negligible change in these pressures due to change in the CO₂ concentration.

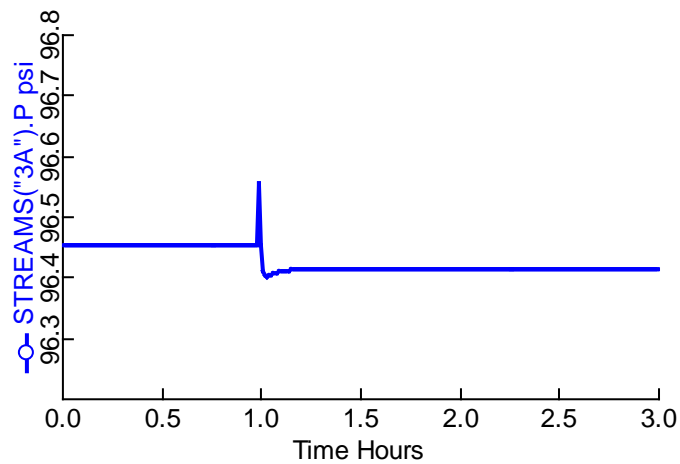


Figure 3-51 Transients in the outlet pressure of the LP section due to step decrease in the CO₂ concentration

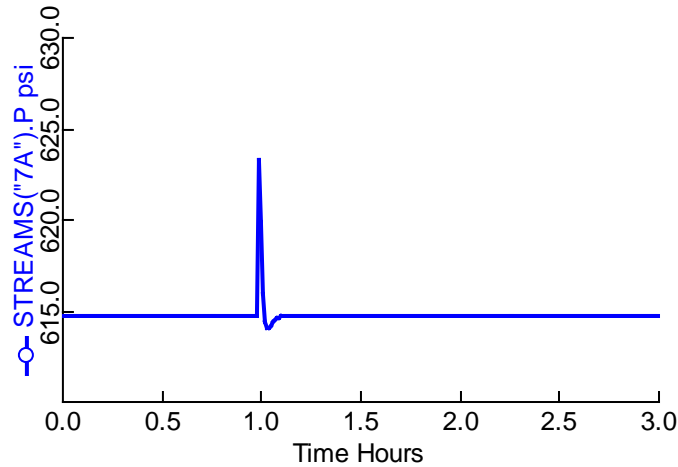


Figure 3-52 Transients in the outlet pressure of the MP section due to step decrease in the CO₂ section

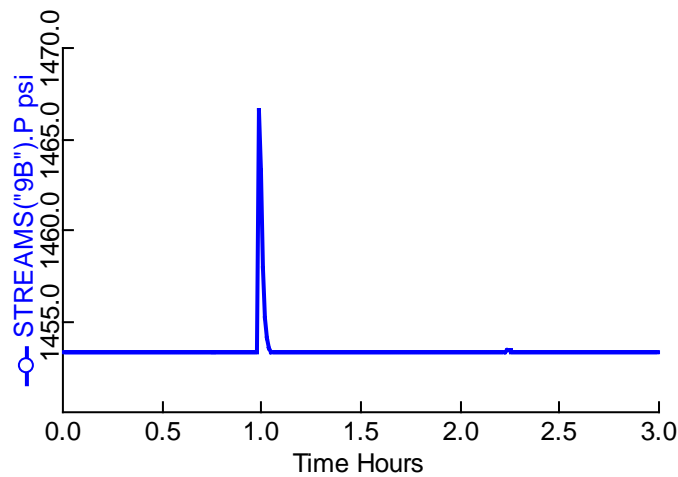


Figure 3-53 Transients in the discharge of the second stage in the HP section due to step decrease in the CO₂ concentration

As the CO₂ concentration decreases, the specific heat at constant pressure (C_p) changes (from 9.214 Btu/lb mol °F to 9.051 Btu/lb mol °F) and the ratio of the specific heats (C_p/C_v) changes (from 1.286 to 1.292). This results in an increase in the compressor discharge temperature. The transient response in the discharge temperature of the HP section (before the cooler) is shown in Figure 3-54.

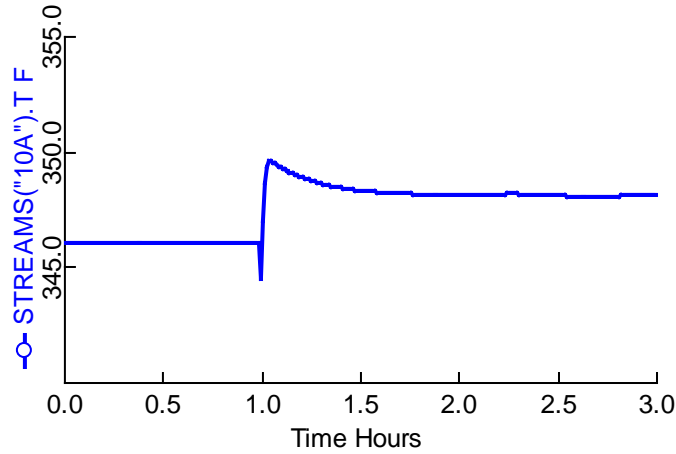


Figure 3-54 Transients in the discharge temperature of the HP section (before the cooler) due to step decrease in the CO₂ concentration

Due to the changes in the fluid properties, it is seen that the decrease in the CO₂ concentration results in an increase in power as seen in Figure 3-55. It should be mentioned that these results strongly depend upon the compressor design as well. The initial overshoot in power consumed is mainly due to the initial overshoot in the flowrate as explained earlier.

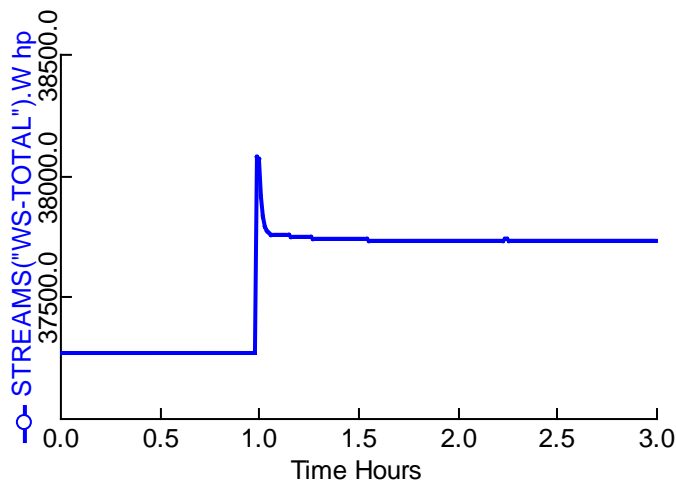


Figure 3-55 Transients of the total power requirement due to step decrease in the CO₂ concentration

4.0 Future plan of work

The following tasks are planned for Year 2.

1. Develop pressure-driven dynamic simulation of bubbling-bed solid-sorbent adsorber reactor for CO₂ capture, starting from flow-driven simulation developed in Year 1
2. Develop pressure-driven dynamic simulation of moving-bed solid-sorbent regenerator reactor
3. Enhance pressure-driven dynamic simulation of CO₂ compression process
4. Develop plant-wide dynamic simulation for generic supercritical pulverized coal (SCPC) power plant in collaboration with Invensys Operations Management (Invensys), along with other members in the team
5. Develop regulatory process controls for bubbling-bed solid-sorbent adsorber reactor for carbon capture
6. Develop regulatory process controls for moving-bed solid-sorbent regenerator reactor
7. Develop regulatory process controls for CO₂ compression model developed from the ACM model
8. Review regulatory process controls implemented for generic SCPC plant (along with other members in the team)
9. Integrate CO₂ capture and compression dynamic models
10. Integrate CO₂ capture/compression dynamic models with APC models (along with other members in the team)
11. Develop software integration plan for modular dynamics/control (along with other members in the team)
12. Complete prototype for one integration option for dynamics/control
13. Perform transient/control studies for coupled solid sorbent-based CO₂ capture/regeneration and compression

4.1 WORK PLAN

Table 4-1 Target dates

Objectives	Due Date
Pressure-driven dynamic simulation of CO ₂ compression process	04/30/12
Pressure-driven dynamic simulation of bubbling-bed solid-sorbent adsorber reactor for carbon capture, starting from flow-driven simulation	06/30/12
Regulatory process controls for CO ₂ compression process	06/30/12
Software integration plan for modular dynamics/control	06/30/12
Regulatory process controls for bubbling-bed solid-sorbent adsorber reactor for carbon capture.	9/30/12
Review regulatory process controls implemented for generic SCPC plant	10/31/12
Pressure-driven dynamic simulation of moving-bed solid-sorbent regenerator reactor.	12/31/12
Regulatory process controls for moving-bed solid-sorbent regenerator reactor.	02/28/13
Complete development for generic SCPC plant dynamic simulation in collaboration with Invensys	12/15/12
Integration of CO ₂ capture and compression dynamic models	12/31/12
Integration of CO ₂ capture/compression dynamic models with APC models	12/31/12
Complete factory acceptance test (FAT) for generic Supercritical plant dynamic simulation	01/15/13
Complete prototype for one integration option for dynamics/control	TBD
Transient/control studies for coupled solid sorbent-based CO ₂ capture/regeneration and compression. Disturbances will include but not be limited to flue gas flowrate variations, flue gas composition variations, and variable CO ₂ capture rates.	01/31/13

5.0 References

1. Pires, J.C.M., F.G. Martins, M.C.M. Alvim-Ferraz, M. Simões. Recent developments on carbon capture and storage: An overview, *Chemical Engineering Research and Design*, Volume 89, Issue 9, September 2011, Pages 1446-1460.
2. Figueroa, J. D., Fout, T., Plasynski, S., McIlvried, H., Srivastava, R. D. Advances in CO₂ capture technology—The U.S. Department of Energy’s Carbon Sequestration Program. *International Journal of Greenhouse Gas Control*, 2 (2008) 9 – 20.
3. Blomen, E., Hendriks, C., Neele, F. Capture technologies: Improvements and promising developments, *Energy Procedia*. Volume 1, Issue 1, February 2009, Pages 1505-1512.
4. Sjostrom, S. and Krutka, H. Evaluation of solid sorbents as a retrofit technology for CO₂ capture. *Fuel* 89 (2010) 1298-1305.
5. Lee, A. Description of Bubbling Fluidised Bed Model, v5.1, 2011.
6. Kunii, D. and Levenspiel, O., *Fluidization Engineering*. First Edition, 1969: John Wiley and Sons.
7. Kunii, D. and Levenspiel, O., *Fluidization Engineering*. Second Edition, 1991: John Wiley and Sons.
8. Introduction to Aspen Custom Modeler®. AspenTech Customer Education Training Manual, Course Number ES250.065.08.
9. Eslick, J., Aspen Plus Model of the CO₂ compression system, e-mail communication on 12/14/2011.